2012-04-18

Skew Effects on Passive Earth Pressures Based on Large-Scale Tests

Shon Joseph Jessee
Brigham Young University - Provo

Skew Effects on Passive Earth Pressures Based on Large-Scale Tests

Shon Joseph Jessee

A thesis submitted to the faculty of
Brigham Young University
in partial fulfillment of the requirements for the degree of

Master of Science

Kyle M. Rollins, Chair
Kevin W. Franke
Fernando S. Fonseca

Department of Civil and Environmental Engineering

Brigham Young University

June 2012

ABSTRACT

Skew Effects on Passive Earth Pressures Based on Large-Scale Tests

Shon Joseph Jessee
Department of Civil and Environmental Engineering, BYU
Master of Science

The passive force-deflection relationship for abutment walls is important for bridges subjected to thermal expansion and seismic forces, but no test results have been available for skewed abutments. To determine the influence of skew angle on the development of passive force, lab tests were performed on a wall with skew angles of 0º, 15º, 30º, and 45º. The wall was 1.26 m wide and 0.61 m high and the backfill consisted of dense compacted sand. As the skew angle increased, the passive force decreased substantially with a reduction of 50% at a skew of 30º. An adjustment factor was developed to account for the reduced capacity as a function of skew angle. The shape of the passive force-deflection curve leading to the peak force transitioned from a hyperbolic shape to a more bilinear shape as the skew angle increased. However, the horizontal displacement necessary to develop the peak passive force was typically 2 to 3.5% of the wall height. In all cases, the passive force decreased after the peak value, which would be expected for dense sand; however, at higher skew angles the drop in resistance was more abrupt than at lower skew angles. The residual passive force was typically about 35 to 45% lower relative to the peak force. Lateral movement was minimal due to shear resistance which typically exceeded the applied shear force. Computer models based on the log-spiral method, with apparent cohesion for matric suction, were able to match the measured force for the no skew case as well as the force for skewed cases when the proposed adjustment factor was used.

Keywords: bridge abutment, passive pressure, skewed abutments, integral abutments, matric suction

ACKNOWLEDGMENTS

I would like to first thank members of my graduate advisory committee Kyle M. Rollins, Kevin W. Franke, and Fernando S. Fonseca for their long hours spent helping with this project and reviewing this thesis. I am grateful to Kyle M. Rollins for the opportunity to work on this project, and also for his exemplary leadership.

I acknowledge and thank the following volunteers who helped with the removal and/or placement of what amounted to more than 80 cubic yards of backfill material throughout the project: Alex Wright, Christina Jessee, Brian Petersen, Nathaniel Whipple, Addison Jenkins, Charles Connors, Brett Anderson, Emily Shepherdson, Travis Fillmore, Scott Christensen, Brent Chase, Greg Riley, Nicholas Riley, Ben Van Noy, Andrew Pratt, Mike Berkey, Cuyler Frisbee, Adam Rose, Elizabeth Alletto, Samuel Mineer, Tanner Christensen, Scott Snow, Alan Snow, Keith Newton, Chad D'Haenens, Danny Paredes, Dillon Hall, Sarah Clark, and Jeremy Fowler. I also acknowledge David Anderson, Rodney Mayo, and their laboratory staff, who assembled and operated the loading and monitoring systems for 17 load tests. I would like to thank my wife, Christina, for the support, encouragement, and assistance she gave as well.

Funding for this study was provided by an FHWA pooled fund study supported by Departments of Transportation from the states of California, Massachusetts, Montana, New York, Oregon, and Utah. This support is gratefully acknowledged.

TABLE OF CONTENTS

LIST OF TABLES

LIST OF FIGURES

1 INTRODUCTION

Passive earth pressures play an important role in soil-structure interaction. They resist lateral movement of structures, and provide stabilizing forces for bridge abutments, laterally loaded piles, sheet pile walls, and anchor blocks. Understanding the behavior of a structure subjected to lateral forces from soil is important for efficient design, and this behavior is often analyzed by evaluating the passive force-deflection curve.

The passive force-deflection relationship for abutment walls is particularly important for bridges subjected to thermal expansion and seismic forces. It gives the magnitude of resistance provided by backfill soil adjacent to an abutment for a given amount of movement. Improved reliability of the passive force-deflection curve will allow for more efficient design.

1.1 Background

Over the past 20 years a number of large-scale tests have been performed to define the passive force-deflection curve which might be expected for dense compacted fill behind bridge abutments (Duncan & Mokwa, 2001; Lemnitzer & Ahlberg, 2009; Maroney, 1995; Rollins & Cole, 2006; Rollins & Sparks, 2002). These tests have generally found that the ultimate passive force is best approximated using the Log Spiral approach and that the maximum force requires a deflection equal to 3 to 5% of the wall height (Cole & Rollins, 2006). The complete passive force-deflection curve can best be estimated by a hyperbolic curve using techniques described by

Shamsabadi, et al. (2007) or by Duncan and Mokwa (2001); however, for design purposes some have recommended a bilinear relationship (AASHTO, 2011; CALTRANS, 2001).

1.2 Limitations of Present Understanding

Although the findings mentioned in the previous section are clearly useful in bridge engineering design, there is considerable uncertainty about their applicability for skewed abutments where passive pressures develop at an angle relative to the longitudinal axis of the bridge structure as shown in Figure 1-1. While many designers consider that the ultimate passive force will be the same for a skewed abutment as for a non-skewed abutment, numerical analyses performed by Shamsabadi et al. (2006) indicate that the passive force will decrease substantially as the skew angle decreases. Reduced passive force on skewed abutments would be particularly important for bridges subject to seismic forces or integral abutments subject to thermal expansion. Unfortunately, there have not been any physical test results for skewed abutments reported in the literature which could guide engineers in making appropriate adjustments for skewed conditions. Nevertheless, some field evidence has suggested poorer performance of skewed abutments during seismic events and distress to skewed abutments due to thermal expansion (Shamsabadi et al., 2006; Steinberg & Sargand, 2010).

To understand better the influence of skew angle on the development of passive force, a series of laboratory tests were performed on a wall that was 1.26 m (4.13 ft) wide and 0.61 m (2 ft) high. A dense sand was compacted behind the wall to simulate a bridge approach fill. Passive force-deflection curves were measured for skew angles of 0º, 15º, 30º, and 45º. This document describes the test program, the test results, and the implications for design practice based on analysis of the test results.

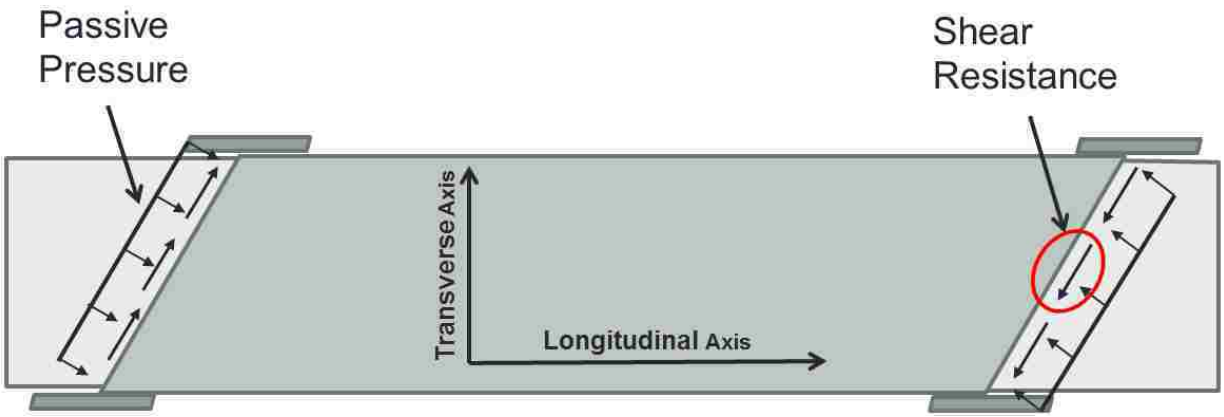

Figure 1-1: Typical Distribution of Forces on a Bridge with a Skewed Abutment due to Thermal Expansion

1.3 Study Objectives

The objectives of this study are as follows:

1. Develop passive force-deflection curves for a concrete backwall against compacted granular backfill for skew angles of 0º, 15º, 30º, and 45º.
2. Determine the effect which the skew angle may have on the ultimate passive force and the shape of the passive force-deflection curve.
3. Investigate the shape of the failure wedge formed behind skewed walls.
4. Develop a procedure for estimating the ultimate passive force as a function of skew angle.

1.4 Scope of Work

A total of nine passive force-deflection tests were performed wherein a concrete backwall having skew angles of 0º, 15º, 30º, and 45º was loaded against dense granular backfill. Tests were performed by pushing the backwall longitudinally into the backfill sand using a hydraulic actuator which was bolted to the backwall. Load was measured directly in the longitudinal, vertical, and transverse directions using load cells. Backwall movement was measured in the

longitudinal, transverse, and vertical directions using string potentiometers. Movements within the backfill including longitudinal compressive strain, vertical heave, and the location of the shear failure surface, were also monitored. Relative compaction of backfill was monitored and controlled to minimize variation in soil shear strength. Moisture levels within the soil were also monitored to account for apparent cohesion due to suction. Passive force deflection curves were developed for each skew angle, and the effect of skew on these curves was evaluated in terms of the ultimate passive resistance, stiffness, and overall curve shape. An equation was developed for computing the passive force for a given skew angle, based on the limited data presently available. Finally, test results were analyzed using both the PYCAP and ABUT software models, as well as the Coulomb Theory for passive pressure.

2 LITERATURE REVIEW

2.1 Introduction

This chapter discusses the current state of knowledge related to passive force-deflection curves for skewed abutments. Topics which will be discussed include:

- passive earth pressure theory;
- integral/semi-integral bridge abutments;
- restraint of skew bridges;
- passive force-displacement curves for non-skew walls; and
- the behavior and performance of skew walls.

The chapter concludes with further discussion of limitations in the state of knowledge which need to be addressed, and how they are addressed in this current study.

2.2 Passive Earth Pressure Theory

Passive earth pressures are pressures which develop when a structure moves laterally into adjacent soil causing compressive strain. Passive pressures are very important in soil-structure interaction problems. They affect the design of many types of structures including soil retaining walls, bridge abutments, deep foundations, and anchor blocks, as is shown in Figure 2-1. To properly account for passive resistance, it is necessary to understand its governing factors, as well as the assumptions and limitations associated with conventional theories.

Figure 2-1: Conditions where Passive Pressures Act on Structures (Duncan & Mokwa, 2001)

2.2.1 Factors Governing Passive Earth Pressures

In a study on passive earth pressures, Duncan and Mokwa (2001) describe four fundamental factors governing the magnitude, the distribution, and direction of passive pressures. These include (1) the amount and direction of the movement; (2) soil strength and stiffness; (3) friction and/or adhesion between the structure and the soil; and (4) the shape of the structure. A brief discussion of these concepts is given below.

2.2.1.1 Movement of the Structure

The movements, forces, and equilibrium requirements for passive pressure conditions are illustrated in Figure 2-2. As a structure moves horizontally, soil moves both upward and horizontally. Due to this upward component of soil movement, an upward force on the wall is applied. If the weight of the structure is large enough to resist this upward force, as is the case

with a laterally loaded pile cap, then these upward forces will fully mobilize. The resultant passive force E_p acting on the structure or wall is thus inclined at an angle δ_{mob} upward from normal to the soil-wall interface. This angle is referred to as the soil-structure interface friction angle or the wall friction. It is important to note that δ is controlled by the amount of movement of the wall in both the vertical and horizontal directions. If the structure is not restrained vertically by either its own weight or by another restraint (e.g. piles below a pile cap), δ may not fully mobilize.

Figure 2-2: Movements, Forces, and Equilibrium Requirements (Duncan & Mokwa, 2001)

The generalized failure mechanism for the case where the wall is restrained vertically involves a wedge-shaped rigid body that slides along a planar slip surface. To satisfy static equilibrium, the resultant force R acting on the failure wedge is oriented at an angle δ_{mob} from normal to the wedge as shown in Figures 2-2 [parts (b) and (c)].

2.2.1.2 Soil Strength and Stiffness

Both the soil strength and stiffness influence the development of passive pressure. A high-strength soil will exert a higher ultimate passive force. A higher level of soil stiffness will result in a higher passive pressure for a given amount of movement. Thus, in order to evaluate passive resistance for a given soil over a range of movements, both of these properties must be properly considered.

2.2.1.3 Interface Friction and Adhesion

As was discussed previously, the resultant passive force acting on the structure is inclined at an angle δ_{mob} inclined upward from normal to the wall face and is called the interface friction angle. A higher interface friction will provide more resistance to the vertical component of the soil's movement. For a vertically constrained structure such as a pile cap supported by piles the magnitude of δ is governed by (1) the nature (roughness) of the interface and the properties of the soil, (2) the amount of relative shear displacement across the interface.

Since δ_{mob} is influenced by both the roughness of the interface and the soil properties, δ_{max} is often described in terms of the ratio δ_{max}/ϕ, where ϕ is the angle of internal friction of the soil. Interface roughness varies with structural material type. Based on a study by Potyondy (1961), conservative values for δ_{max}/ϕ were developed for common structural materials and are given in Table 2-1.

Table 2-1: Minimum Values for δ_{max}/ϕ (Potyondy, 1961)

	Structural Material		
Soil type	Steel (δ_{max}/ϕ)	Concrete (δ_{max}/ϕ)	Wood (δ_{max}/ϕ)
Sand	0.54	0.76	0.76
Silt and clay	0.54	0.50	0.55

As was noted previously, when a vertically constrained structure such as a pile cap is loaded laterally against soil, the interface friction δ_{mob} will begin to mobilize at the wall-soil interface. As the wall continues to move, this interface friction will continue to develop until a peak value δ_{max} is reached. The amount of relative shear displacement required for δ to fully mobilize to the level of δ_{max} is typically very small, around 0.1-0.25 in (Duncan & Mokwa, 2001). Magnitudes of displacement smaller than this range will result in only partial δ mobilization.

For cohesive soils, the soil's adhesion to the wall c_a can also provide resistance to shearing at the soil-structure interface. This adhesion is usually characterized in terms of $\alpha = c_a/c$, where c is the soil's cohesion. Typical values for α range from about 0.5 for stiff soils to about 0.9 for soft soils (Duncan & Mokwa, 2001).

2.2.1.4 Structure Shape

Figure 2-3 illustrates the failure surface in three dimensions for a wall of finite length. In conventional theory, passive resistance is modeled based on plane strain or 2D geometry for a wall of infinite length. However, since no walls have infinite length, the ends of a wall have an effect on the development of passive pressure. This effect is manifested in the geometry of the failure plane in Figure 2-3. Referring to this figure, passive pressures acting the wall transition from two-dimensional at cross section A-A to three-dimensional at the wall ends. A greater volume of soil per unit wall length is displaced at the wall ends than is displaced at the center of the wall. This results in greater passive resistance per unit wall length than in the case for an infinite wall length. These end effects or "3D effects" can be significant, and should be accounted for. A procedure for accounting for end effects is proposed by Brinch Hansen (1966)

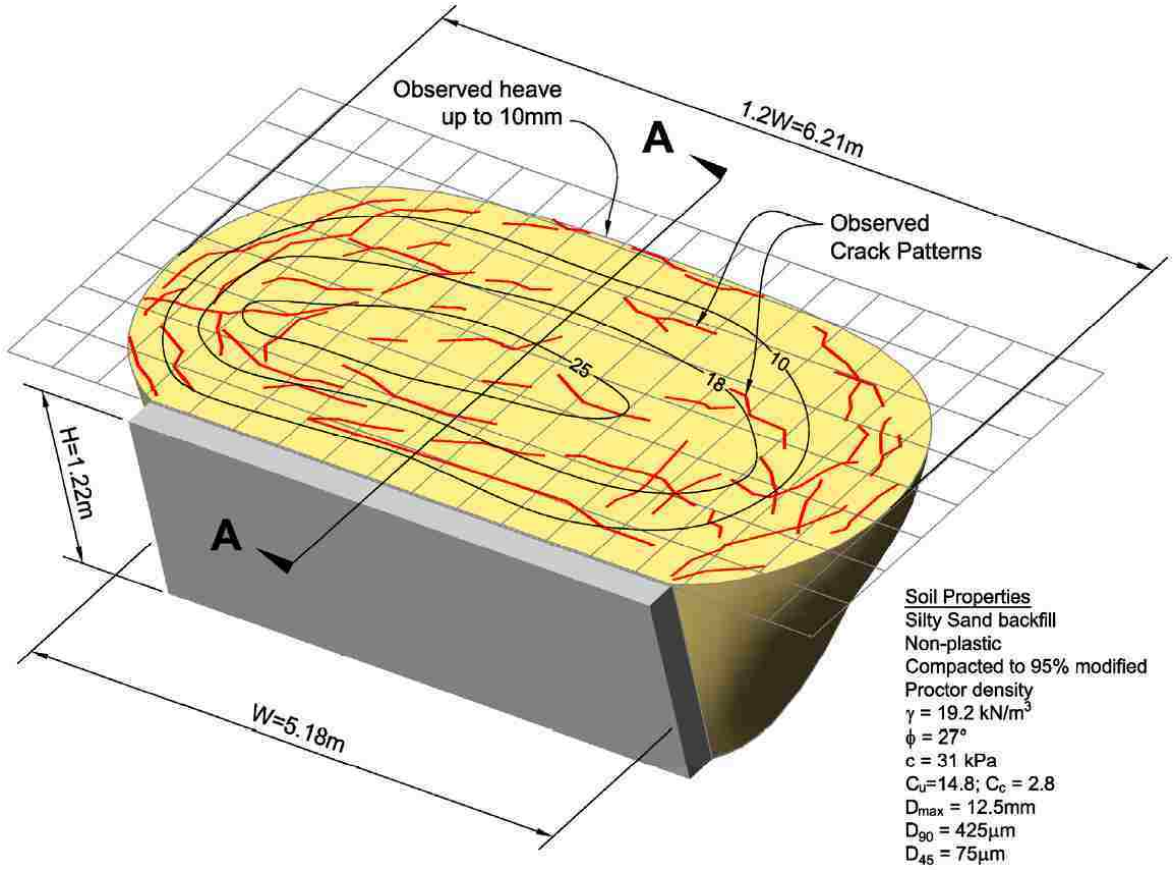

Figure 2-3: Diagram Showing a Typical Three-Dimensional Passive Pressure Failure Surface [Shamsabadi, 2006 (after Rollins and Cole (2006)]

Ovesen (1964) conducted a series of passive pressure tests and found that passive pressures associated with structures of lesser length are higher than those predicted by conventional theory. Brinch Hansen (1966) developed a method for correcting the results of conventional passive pressure theories for shape effects. The correction factor can range from 1.0 for a wall of infinite length to an upper limit of 2.0 for smaller structures. The Brinch Hansen method for correcting for 3D effects is further discussed in Duncan and Mokwa (2001).

2.2.2 Conventional Passive Pressure Theories

Various theories have been developed for computing passive resistance, and have been used for hundreds of years. These theories are all based on the same general equation. For a given wall loaded laterally against horizontal backfill soil, passive pressure varies proportionally with the wall height. The passive pressure, σ_p, at a given depth z below the top of the wall is given by the equation

$$\sigma_p = 0.5\,\gamma\,z\,K_p + 2\,c'(K_p)^{0.5} \tag{2-1}$$

where γ is the unit weight of the backfill, K_p is the coefficient of passive earth pressure, and c' is the effective cohesion of the soil. Since passive pressure varies with depth, it is conveniently expressed as a passive force P_P given by the equation

$$P_P = 0.5\,\gamma\,B\,H^2\,K_p + 2\,c'\,B\,H\,(K_p)^{0.5} \tag{2-2}$$

where B and H are the wall width and height, respectively. Conventional theories for computing K_p are described in this section. Equation 2-2 consists of two components: (1) the passive resistance due to the unit weight of the backfill; and (2) the passive resistance due to backfill cohesion. It should be noted that the unit weight component acts at a distance $H/3$ above the bottom of the wall, and is oriented at an angle δ to the wall as illustrated in Figure 2-2. The cohesive component acts at a distance $H/2$ above the bottom of the wall. Cohesion is relatively minor for granular backfills and is often ignored, thus leading to a height of $H/3$ at which the resultant force acts.

2.2.2.1 Rankine, Coulomb Theories

The Rankine Theory (Rankine, 1857) and the Coulomb Theory (Coulomb, 1776) are two long-standing and widely used theories today in geotechnical engineering. The Rankine Theory is based on stress states at failure specified according to the Mohr-Coulomb failure criteria. The Coulomb Theory is a limit equilibrium theory wherein forces are evaluated for different possible failure wedges until a global minimum resistance is found. Because the Coulomb Theory treats passive pressure as a limit equilibrium problem, it is an upper-bound theory. The Rankine Theory, on the other hand, is a lower bound theory since it is based on a lower bound failure criterion. The Coulomb Theory accounts for soil-wall interface friction δ and Rankine does not, assuming that the interface friction is zero. Because of this, the Coulomb Theory yields higher and usually more realistic K_p values than the Rankine Theory, often making it more preferable over the Rankine Theory. It should be noted, however, that for wall friction greater than about 0.4ϕ, the Coulomb Theory overestimates passive force. Both theories assume a planar failure surface.

2.2.2.2 Log Spiral Theory

The logarithmic spiral (Log Spiral) earth pressure theory is not as widely used as the Rankine and Coulomb theories, but it is generally agreed to be the most accurate theory for passive pressures based on experience with large-scale tests (AASHTO, 2011; Duncan & Mokwa, 2001). Like the Coulomb Theory, it is based on limit equilibrium, and is thus an upper-bound theory. The general method for computing passive pressures using the Log Spiral Theory is the graphical procedure. This procedure is based on the failure mechanism shown in Figure 2-4, and is explained in greater detail in Terzaghi (1943) and Terzaghi and Peck (1996). This procedure is considerably complex, requiring an iteration process to define the critical failure

surface. It is therefore most commonly employed using either charts or numerical analysis. Figure 2-4 illustrates how the failure surfaces vary according to the magnitude of the wall friction angle relative to the soil friction angle, according to the Log Spiral approach.

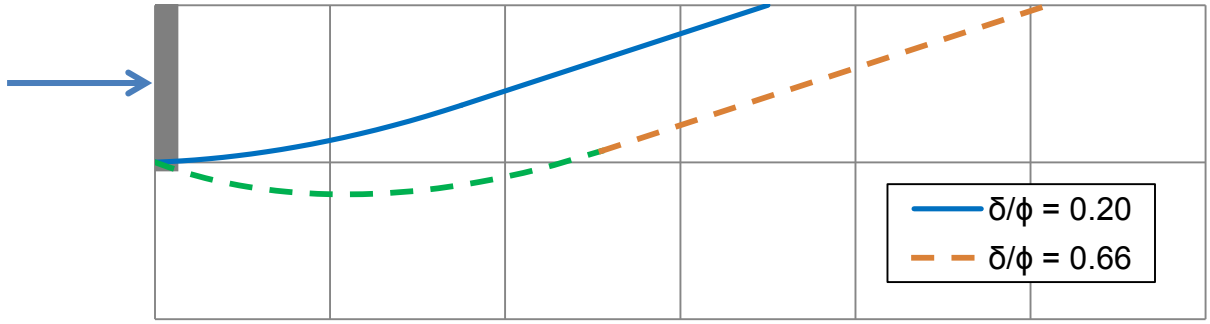

Figure 2-4: Log Spiral Failure Mechanism for Different Magnitudes of Wall Friction

In comparing the Coulomb Theory with the Log Spiral Theory, there is very little difference for conditions where the interface friction δ is less than 40% of the soil's internal friction angle ϕ. The Coulomb Theory is a reasonably accurate method for evaluating passive pressures under these conditions. However, for conditions where the interface friction δ exceeds 0.4ϕ, the Coulomb theory becomes very sensitive to interface friction and the computed passive resistance is substantially higher. This is because the Coulomb Theory assumes that the passive pressure failure mechanism involves a planar slip surface, whereas the Log Spiral Theory assumes what is often a more probable failure mechanism. Furthermore, the Log Spiral Theory has been observed to have good agreement with load tests for conditions where interface friction is high (Duncan & Mokwa, 2001; Rollins & Cole, 2006). It is thus generally agreed to be the most accurate method for evaluating passive pressures.

2.2.2.3 Other Theories

Several other alternative procedures for evaluating K_p have been developed which generally confirm the accuracy of the Log Spiral Theory (Chen & Su, 1994; Kumar & SubgaRao, 1997; Soubra, 2000; Zhu & Qian, 2000). These are numerical procedures, and are all based on limit equilibrium of forces and plasticity theory.

Understanding the passive forces from backfill soil generated during an earthquake is also important for bridges and other structures. Because seismic passive loading is extremely complicated, and because documented case histories of the performance and response of actual structures is very limited, most of the current understanding of this type of loading has come from model tests and numerical analyses (Kramer, 1996). Okabe (1926) and Mononobe and Matsuo (1929) developed the basis for a simplified numerical method to approximate seismic passive pressures for walls with larger displacements (also known as "yielding walls"). This theory essentially applies the Coulomb Theory under pseudo-static conditions wherein the total passive thrust generated by backfill soil undergoing positive horizontal acceleration is approximated. Steedman and Zeng (1990) developed a similar pseudo-static method which also accounts for phase difference and amplification effects within the backfill. More recently, SubbaRao and Choudhury (2005) also proposed a pseudo-static approach for evaluating passive resistance generated by seismic loading.

Methods for computing the passive force-deflection curve relationship are also available. These theories commonly estimate this curve using a hyperbolic model, and typically are governed by input parameters such as the ultimate passive force, soil stiffness, and displacement required for ultimate passive force to develop. Hyperbolic curves by Shamsabadi et al. (2007) and Duncan and Mokwa (2001) are two effective methods. However, for design purposes some

have recommended a bilinear relationship (AASHTO, 2011; CALTRANS, 2001). This bilinear representation of the passive force-deflection curve is illustrated in Figure 2-5, and consists of forming two lines: one line extends from the origin to a deflection of about 0.01 to 0.02*H* at the ultimate passive force, and the second line continues horizontally from the top of the first line. None of these procedures account for the drop to residual strength that often occurs after the peak strength.

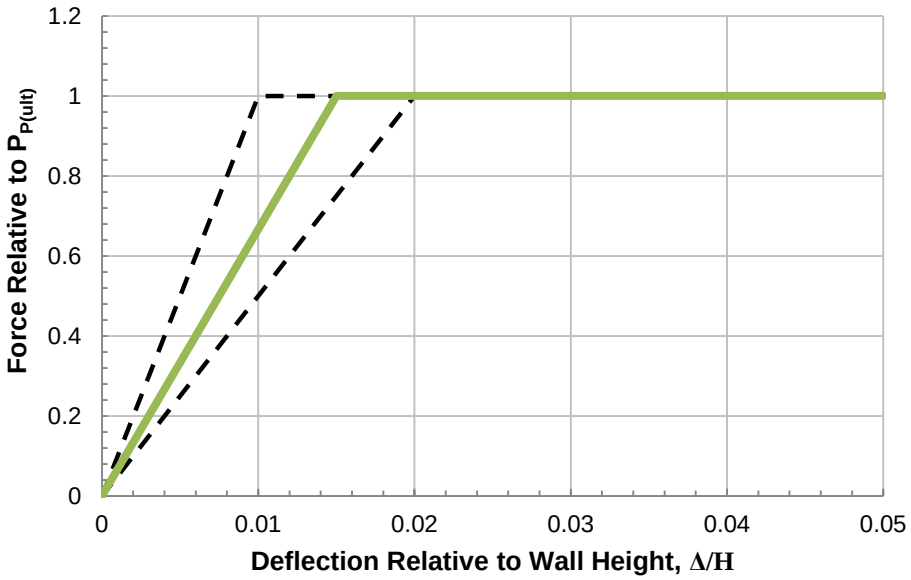

Figure 2-5: Illustration of the Bilinear Relationship Proposed by AASHTO (2011)

2.2.3 Integral/Semi-Integral Bridges

The purpose of this section is to discuss important modes of bridge design that are currently used and the importance of passive resistance from structural backfill in these designs. Integral bridge construction has become increasingly popular over the past several decades, and even more so during the last 15 years (Dunker & Liu, 2007).

An integral bridge is constructed as a frame so that the superstructure (girders, deck, and diaphragm) are connected to the foundation at the diaphragm-abutment interface (Steinberg et al., 2004). This bridge type is also commonly referred to as a "jointless" bridge because of the elimination of the thermal expansion joint commonly seen on older bridges. With an expansion joint, a bridge is subject to higher rates of corrosion as salt water enters the joint. Elimination of the expansion joint has lowered maintenance costs and the overall integral design is more efficient in terms of construction costs, construction time, durability, and the overall life cycle costs.

Integral bridges are constructed so that the foundation is more flexible. This is done so that the foundation will deflect as the superstructure expands during periods of warmer temperature. When this occurs, high levels of pressure can develop behind the abutment wall. Although the flexibility of the foundation allows for movement, some bridges of large lengths or large skew angles require more movement than that allowed by the foundation. Thus, to minimize the use of the conventional expansion joint, the more flexible semi-integral bridge concept was developed for these conditions (Steinberg & Sargand, 2010).

Semi-integral bridges are similar to integral bridges in that there is no expansion joint on the bridge deck. The difference is the addition of a moveable joint with elastomeric bearings at the interface between the diaphragm and the foundation. Thus, only the top portion of the foundation wall actually moves into the adjacent structural backfill as the superstructure expands. A typical semi-integral bridge profile is illustrated in Figure 2-6.

2.3 Bridge Movements and Forces

With the development of the jointless bridge, the pressures behind the bridge end diaphragm vary with different levels of bridge expansion. In skew bridges these pressures can

compromise rotational stability without proper restraint. While many bridges are designed with longitudinal, lateral, and vertical restraints, skew bridges subjected to thermal expansion require rotational restraint as well. Appropriate restraint will allow for optimized functionality of the bridge (Burke, 1994).

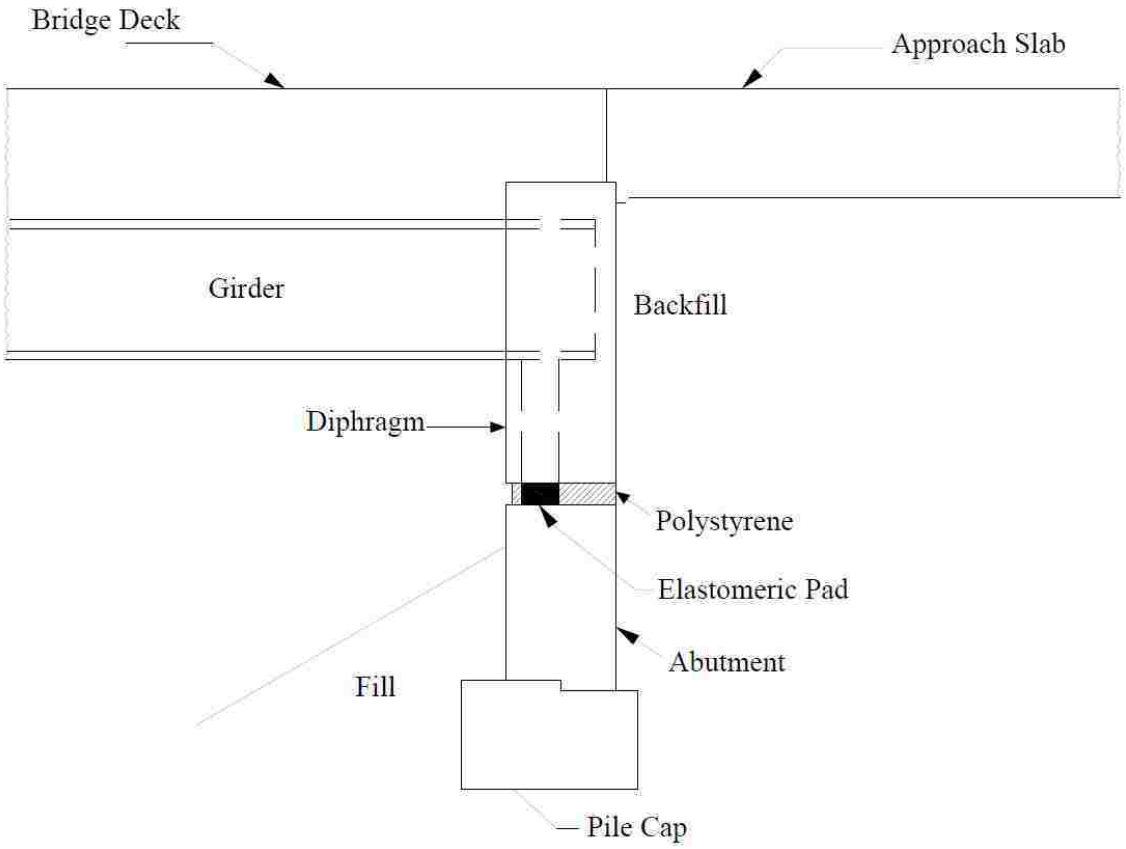

Figure 2-6: Typical Semi-Integral Bridge Profile (Steinberg & Sargand, 2010)

Bridges are designed with longitudinal, lateral, vertical, and sometimes rotational restraint. Burke (1994) describes various sources of longitudinal and lateral restraint for the superstructure of a semi-integral bridge. Sources of longitudinal restraint include friction between the approach slab and the subbase, shearing resistance of elastomeric bearings, and passive resistance of structural backfill. Lateral restraint is provided essentially by

superstructure-backfill-approach slab interaction, and shearing resistance of elastomeric bearings in bridge seat joint. Steinberg and Sargand (2010) showed that wingwalls can be an additional source of lateral restraint for a semi-integral bridge.

Rotational restraint applies primarily to skewed bridges. Bridge geometry (bridge skew angle, deck width and height) greatly affects the overall mechanism for rotation and thus should be considered in evaluating rotational restraint. In longer, narrower bridges, guide bearings and wingwalls may play a more important role in resisting rotation for a given skew angle; whereas shorter, wider bridges will typically resist rotation primarily with friction from wall-backfill interaction behind the end diaphragm (Shamsabadi et al., 2006). The tendency to rotate increases with skew angle, and this rotation will initiate sooner for longer bridges (Burke, 1994).

The distribution of forces at the interface between a skewed bridge and the adjacent backfill soil is illustrated in Figure 2-7 as originally outlined by Burke (1994). The longitudinal force P_L can be produced by thermal expansion or seismic forces. The components of the longitudinal force normal and transverse to the abutment must be resisted by the passive force P_P normal to the abutment backwall and the shear resistance P_R on the backwall. Summing forces normal to the abutment produces the equation

$$P_P = P_L \cos\theta \tag{2-3}$$

where θ is the skew angle of the backwall.

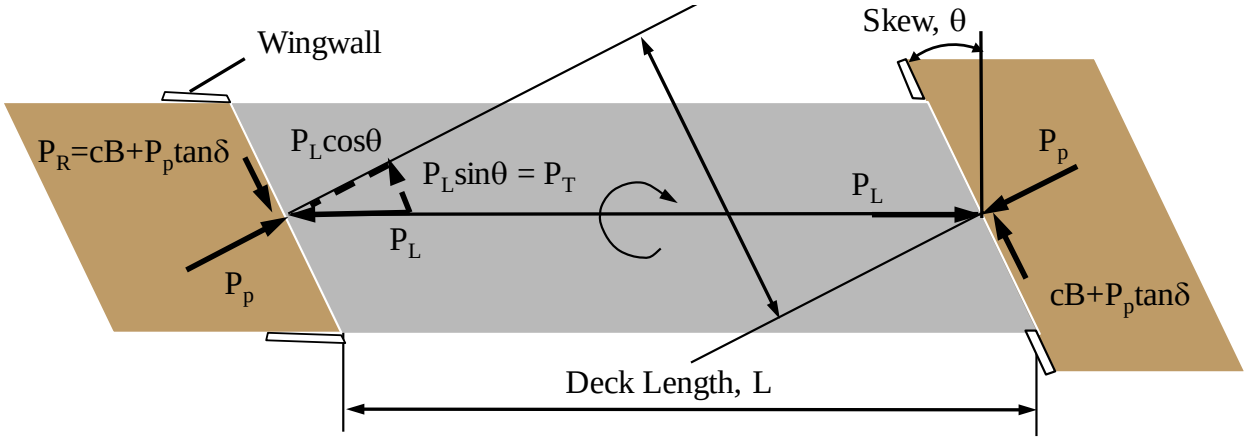

Figure 2-7: Typical Distribution of Forces on a Bridge with a Skewed Abutment

The transverse applied shear force P_T can be computed using the equation

$$P_T = P_L \sin\theta \tag{2-4}$$

while the transverse shear resistance P_R can be given by the equation

$$P_R = c\,B\,H + P_P \tan\delta \tag{2-5}$$

Summing forces transverse to the backwall produces the equation

$$(cA + P_P \tan\delta) / F_s \geq P_L \sin\theta \tag{2-6}$$

where c is the soil cohesion, B is the backwall width, H is the backwall height, δ is the angle of interface (or wall) friction between the backfill soil and the concrete abutment backwall, and F_s

is a factor of safety. If the applied transverse shear resistance exceeds the ultimate shear resistance, the abutment could slide against the soil, leading to an unstable condition.

In addition, the offset in passive force on the abutments produces a force couple which must be resisted by the force couple produced by the shear resistances on each abutment. Summing moments about a vertical axis leads to the equation

$$(cA + P_P \tan\delta)\, L \cos\theta / F_s \geq P_P L \sin\theta \tag{2-7}$$

Again, if the shear resistance is insufficient, the bridge will tend to rotate, which would likely change the distribution of passive force on the abutments. Based on Equation 2-7, Burke (1994) suggested that rotation would be expected for skew angles greater than 15º with smooth abutment-soil interfaces and no cohesion if the factor of safety dropped from 1.5 to 1.0. If cohesion is ignored, the potential for rotation is independent of both P_P and the length of the bridge, L; Equation 2-7 thus can be simplified to

$$\theta \leq \tan^{-1}(\tan\delta / 1.5) \tag{2-8}$$

For concrete structural material with typical interface friction angle δ of 22° (Burke, 1994), Equation 2-8 suggests that for a skew angle θ greater than 15° the bridge will become unstable. However, this is a conservative estimate since wall friction values greater than 22° have been reported in the literature (Rollins and Cole (2006) reported a wall friction of 30° for clean sand, and according to Table 2-1, a clean sand will have a minimum δ/ϕ ratio of 0.76).

2.4 Passive Force-Displacement Tests for Non-Skew Walls

Over the past 20 years a number of large-scale tests have been performed to define the passive force-deflection curve which might be expected for dense compacted fill behind bridge abutments (Duncan & Mokwa, 2001; Lemnitzer & Ahlberg, 2009; Maroney, 1995; Rollins & Cole, 2006; Rollins & Sparks, 2002). These tests have generally found that the ultimate passive force requires a deflection equal to 3 to 5% of the wall height, and have been important for developing models for approximating passive force-deflection curves. A few of these more recent and studies are discussed below.

2.4.1 Maroney (1995)

Maroney (1995) performed two large-scale tests on end-diaphragm backwalls having different geometry and soil types. The two tests were performed simultaneously using hydraulic rams mounted between the two walls, with clayey silt used as embankment fill on one side, and well- to medium-graded sand used on the other side. The backwalls were supported by piles, and deflection of the wall occurred with hinge-type behavior in the pile, rather than translational movement. The qualitative load-deflection behavior was observed to be remarkably similar for both tests in terms of backfill stiffness despite the differing soil types and wall geometries. The normalized passive force-deflection curves for each test are shown in Figure 2-8. The load deflection-curve was initially computed using a curve fitting technique which uses a dimensionless polynomial to relate passive resistance to wall deflection. Results from these tests were used to improve the calibration of this polynomial for improved future use. The resulting predicted and adjusted polynomial curves are also shown in Figure 2-8. This test is the source of the 5 ksf uniform pressure distribution specified in the latest Caltrans seismic design code (CALTRANS, 2010) and in the AASHTO code (AASHTO, 2011) for cohesive soils.

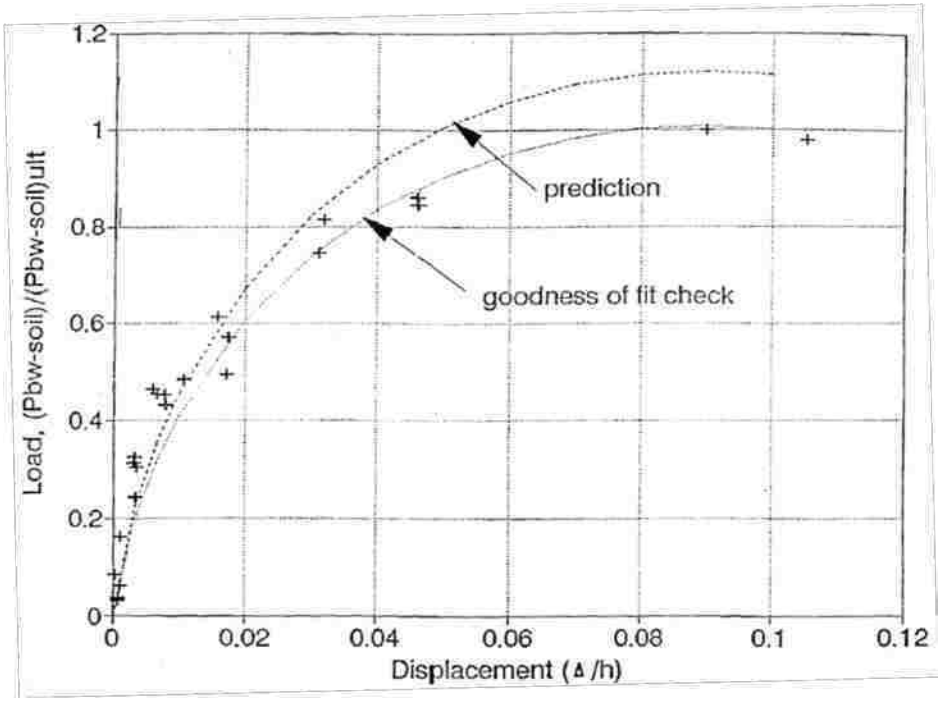

Figure 2-8: Plot of Predicted and Measured Passive Force Deflection Curves (Maroney, 1995)

These and other various recent studies have helped to improve understanding of the passive force-deflection behavior of walls under various conditions. Rollins and Sparks (2002) gave a comprehensive summary of medium to large-scale tests performed on dense sand. This summary is provided in Table 2-2.

2.4.2 Duncan and Mokwa (2001)

Duncan and Mokwa (2001) performed two load tests on a 1.07 m (3.5 ft) tall by 1.92 m (6.3 ft) wide anchor block using both the natural ground and compacted gravel as backfill material. The natural soil at the site was desiccated hard sandy silt (ML) and sandy clay (CL). The gravel backfill used for the second test was crushed aggregate (GW-GM and SW-SM) compacted to about 80% relative density. The strength parameters and soil unit weight for both soil types are given in Table 2-3, and the test arrangement is shown in Figure 2-9.

Table 2-2: Chronological Summary of Medium to Large-Scale Passive Pressure Test Results (Rollins & Sparks, 2002)

Reference	Material properties	Wall height	Mode of movement	$\Delta H/H$
Terzaghi (1934)	Dense uniform medium grain angular sand, $e=0.66$, $D_r=79\%$, $\phi\approx47°$, $\delta=6°$, Compacted.	2.13 m	Rotation about base	0.001[a]
Tschebotarioff and Johnson (1953)	Medium grain sand, Dense: $e=0.58$, $D_r=85\%$, $\phi\approx42\%$, $\delta\approx21-35°$; Loose sand: $e=0.71$, $D_r=37\%$, $\phi\approx39\%$; placement by raining through hose followed by hand tamping.	610 mm	Translation	Dense: 0.05–0.06 Loose: >0.18
Schofield (1961)	Dense medium grain sand, $e=0.58$, $\phi\approx44°$; placement by raining through hose, no vibration or tamping.	150 mm	Rotation about top	0.048
Rowe and Peaker (1965)	Dense fine sand, $e=0.58$, $\phi\approx42°$ Plane Strain, $\delta\approx27°$, placement by raining with no vibration	450 mm	Translation	0.04–0.07
Mackey and Kirk (1968)	Dense fine, medium and coarse sands, $e=0.62$, 0.49, 0.53, $D_r=75$, 76, 85%, $\delta\approx22°$, 25.5°, 17°, $\phi\approx50°$, placement by raining with some vibratory compaction	300 mm	Translation	0.016–0.025
Narain et al. (1969)	Dense fine sand, $\phi\approx42°$ $D_r=70\%$, $\delta\approx23.5°$, placement by raining with hand tamping compaction	450 mm	Translation Rotation about top Rotation about base	0.033–0.075 0.02–0.06 0.07–0.10
Broms and Ingelson (1971)	Dense sand, $e=0.59$, $D_r=82\%$, $\phi\approx33°$, $\delta\approx23.5°$, placement by 3.8 t vibratory roller compaction.	2.75 m	Rotation	0.0013–0.0017[b]
Tcheng and Iseux (1972)	Dense uniform clean fine sand, $\phi\approx38-40°$	3.0 m	Rotation	0.02–0.06
Carder et al. (1977)	Dense uniform medium grain sand, $e=0.31$ $\phi\approx39°$, $\delta\approx15-21°$, compacted in 0.15 m layers with vibratory drum roller.	1.0 m	Translation	0.025
Maroney (1995)	Well-graded coarse to medium grain sand, placement by pluviation to 92–95° of mod. Proctor density $e=0.4-0.46$, $\phi\approx41°$, Field Test	2.06 m	Translation	>0.025
Duncan and Mokwa (2001)	Dense crusher run gravel, $D_r=80\%$, $\phi\approx48-52°$, $\delta\approx6°$, Compacted, Field Test	1.067	Translation	0.03

[a]Passive pressure not fully mobilized $K_p=2-2.5$.

[b]Rankine passive pressure only mobilized $K_p<3.3$.

Table 2-3: Backfill Soil Properties for Load Tests Performed at the Virginia Polytechnic Institute Field Test Site (Duncan & Mokwa, 2001)

Soil	Properties		
	c (psf)	ϕ (°)	γ (pcf)
Natural soil	1000	32-38	122-135
Gravel backfill	0	48-52	135

Figure 2-9: Layout of Tests Performed at the Virginia Polytechnic Institute Field Test Site (Duncan & Mokwa, 2001)

In both tests, the block was loaded incrementally to failure, and loads were measured directly using a columnar load cell. Deflection of the block was measured using cable position transducers, and the block was observed to move both horizontally and upward with the soil in both tests. The measured ultimate passive resistance exhibited by the natural soil was 138 kips, and the resistance the resistance exhibited by the gravel backfill was 92 kips at a maximum deflection of about 1.5 in. Since gravel is typically considered to be the ideal backfill material in terms of strength, it was expected that the gravel would exhibit greater passive resistance than

the natural soil. However, higher resistance measured in the natural soil was not surprising considering the relatively low confining pressures exerted on the gravel, and also considering the high strength of the in-situ soil due to desiccation and its considerable cohesion. The distance from the top of the wall to failure plane location at the ground surface for the native soil and gravel reached 2.1 m (6.0 ft) and 2.4 m (7.0 ft), respectively as shown in Figure 2-10. The peak load corresponded to a displacement of about 1.5 in. for each test, which is about 3.6% of the wall height.

The results from the two tests were compared with computed results using the Rankine, Coulomb, and Log Spiral theories (with and without correction for 3D effects). The best agreement with test results was achieved using the Log Spiral Theory. The computed passive force-deflection curve is a hyperbolic curve constructed using techniques described by Duncan and Mokwa (2001), and is a function of ultimate passive resistance, deflection, initial slope of the load-deflection curve, and a failure ratio coefficient. Computed and measured passive force-deflection curves for the two cases are shown in Figure 2-11.

2.4.3 Rollins and Sparks (2002)

Rollins and Sparks (2002) generated the passive force-deflection curve during a static lateral load test on a 3 × 3 pile group. The piles were driven in low-plasticity silt and clay soil, and sandy gravel backfill was placed to provide lateral resistance at the side of the pile cap. The passive force-deflection curve for this test condition was estimated using the hyperbolic relationship given in Duncan and Mokwa (2001), and curves were developed based various passive pressure theories. A plot of measured and computed curves is shown in Figure 2-12. The Log Spiral theory showed the best agreement with the measured results.

Figure 2-10: Failure Surface Geometry (Duncan & Mokwa, 2001)

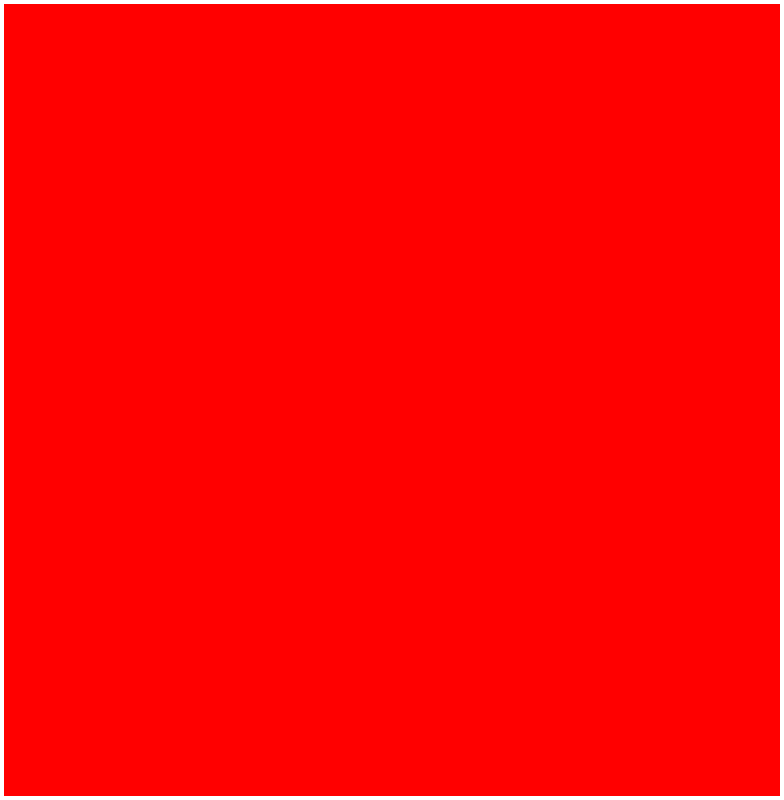

Figure 2-11: Computed and Measured Passive Force-Deflection Curves (Duncan & Mokwa, 2001)

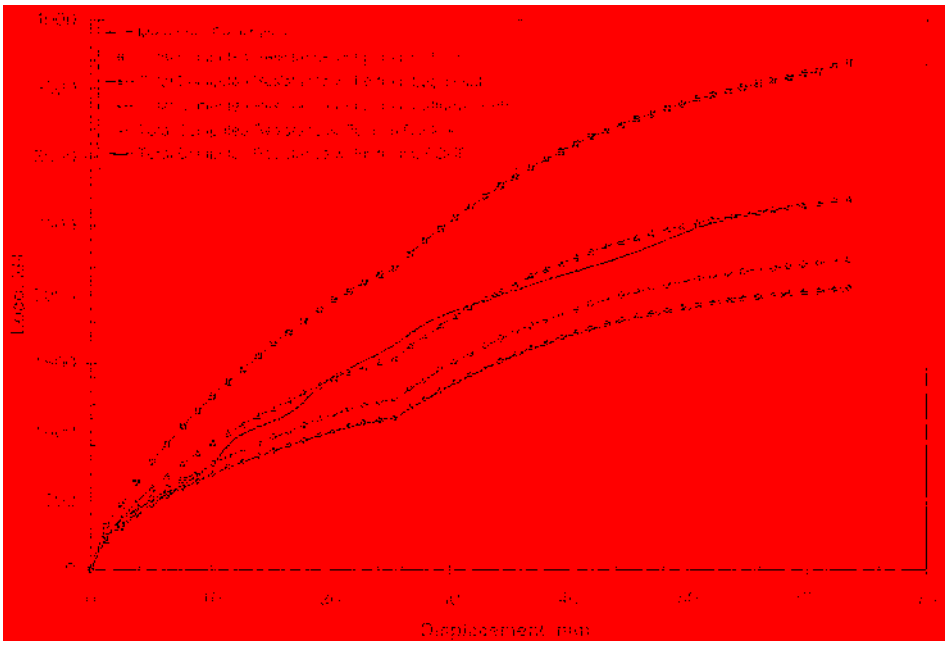

Figure 2-12: Measured and Computed Passive Force-Deflection Curves (Rollins & Sparks, 2002)

2.4.4 Rollins and Cole (2006)

Rollins and Cole (2006) performed full-scale lateral load tests on a 4 × 3 pile group driven into a cohesive soil profile. The pile cap was 5.18 m long, 3.05 m wide and 1.12 m high. The passive resistance was measured from four tests with four different soil types, including clean sand, silty sand, fine-grained gravel, and coarse-grained gravel. The soil properties of these backfill types are provided in Table 2-4, and a summary of the test results are provided in Table 2-5. The coarse gravel provided the greatest amount of passive resistance, followed by the silty sand, clean sand, and fine gravel. The passive force-deflection curve for each backfill type is provided in Figure 2-13. The ultimate passive resistance typically occurred at a normalized wall deflection of 3 to 5% of the wall height. The failure surface for each test was in good agreement with that predicted by the Log Spiral Theory.

Table 2-4: Summary of Backfill Soil Properties from Full-Scale Load Tests (Rollins & Cole, 2006)

Backfill type	Moisture content $w[\sigma]^a$ (%)	Dry unit weight $\gamma_d[\sigma]^a$ (kN/m^3)	SRC[b] (%)	MRC[b] (%)	D_r (%)	ϕ (deg)	c (kPa)	δ/ϕ
Clean sand	13.4 [1.74]	16.18 [0.26]	98	93	63	39	0.0	0.77[e]
Silty sand	14.6 [2.13]	16.57 [0.27]	98	93	67[d]	27	27.3	0.75[d]
Fine gravel	5.5 [0.43]	19.68 [0.47]	98	91	54[c]	34	3.8	0.75[d]
Coarse gravel	4.0 [0.86]	22.23 [0.60]	103	94	69[c]	40	7.2	0.75[d]

[a]Mean and standard deviation (σ).

[b]Standard Proctor (SRC) and Modified Proctor (MRC) relative compaction, where RC=$\gamma_{d\ field}/\gamma_{d\ max}$.

[c]Estimated using correlations Lee and Singh (1971).

[d]Estimated value, assuming no adhesion (intercept).

[e]Measured value with no adhesion.

Table 2-5: Summary of Backfill Testing Results (Rollins & Cole, 2006)

Backfill soil type	Peak passive force, P_{ult} (kN)	Pile cap deflection at peak passive force, Δ_{max} (mm)	Normalized pile cap deflection, Δ_{max}/H	Passive force contribution to pile cap resistance at Δ_{max}/H (%)
Clean sand	1090	38	0.034	40
Silty sand	1428	58	0.052	33
Fine gravel	774	34	0.03	33
Coarse gravel	1997	39	0.035	47

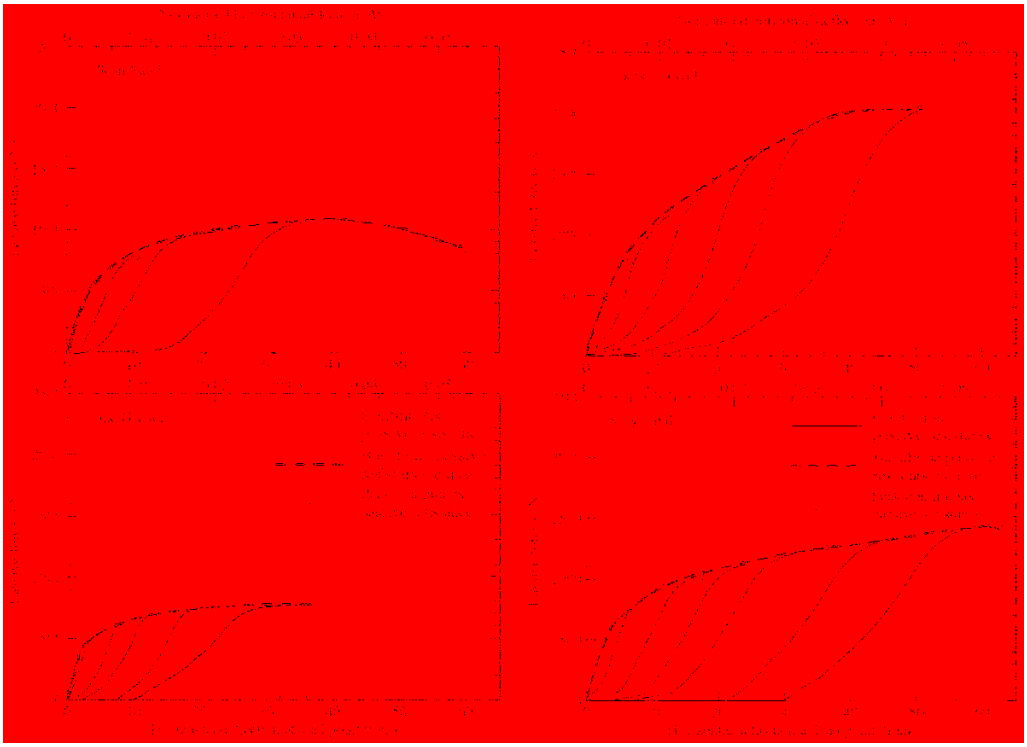

Figure 2-13: Computed first Cycle and Backbone Passive Force-Deflection Curve (Rollins & Cole, 2006)

2.4.5 Lemnitzer and Ahlberg (2009)

Lemnitzer and Ahlberg (2009) performed full-scale cyclic lateral load tests on an abutment backwall having dimensions, backfill conditions, and boundary conditions typical of those had by highway bridges in California. The ultimate passive resistance occurred at a displacement of 0.03H and corresponded to a passive earth pressure coefficient of 16.3. The soil backfill was a well-graded sand with silt with a cohesion between 14 and 24 kPa, and the soil-wall interface friction angle was 33 to 50% of the internal soil friction angle. The measured passive resistance was in good agreement with computed passive resistance using the Log Spiral Theory, and the shape of the force-deflection curve was computed using the hyperbolic relationship given by Duncan and Mokwa (2001). Figure 2-14 shows both the measured and computed curves. The LSH curve shown in Figure 2-14 is based on the method of slices, and is estimated using the Log Spiral Hyperbolic (LSH) model developed by Shamsabadi et al. (2007).

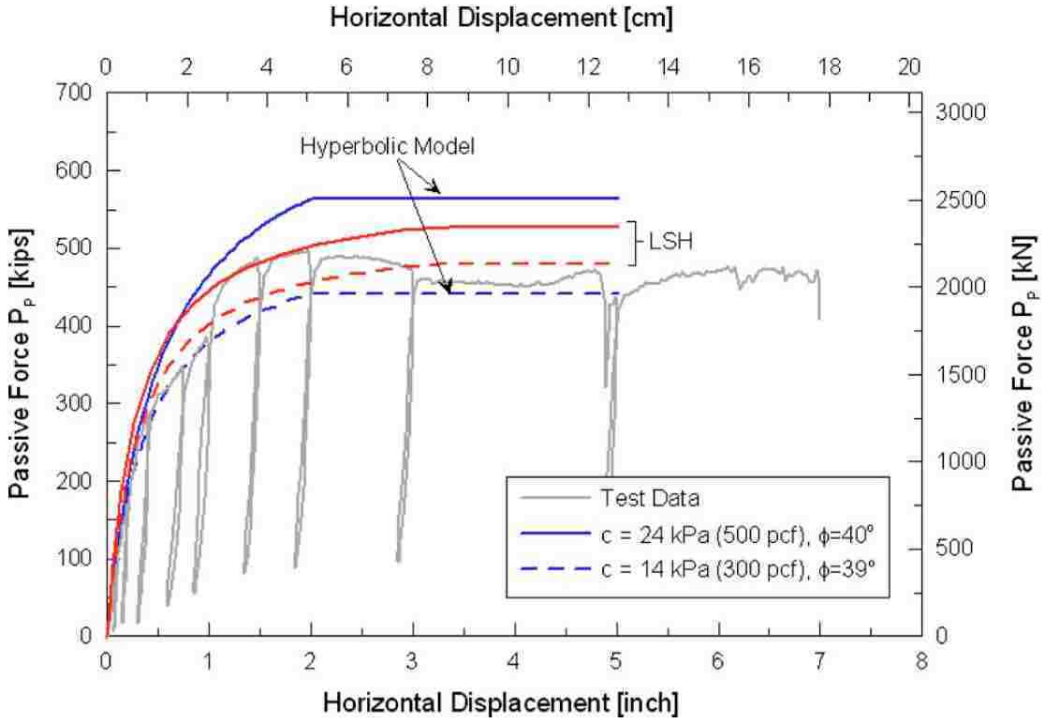

Figure 2-14: Measured and Computed Passive Force-Deflection Curves (Lemnitzer & Ahlberg, 2009)

2.5 Behavior/Performance of Skew Walls

Although no large-scale passive force-deflection tests have been performed on skewed walls, various researchers have evaluated the behavior and performance of skewed abutments to understand better the effects of skew on soil pressures behind integral abutments. In a study by Sandford and Elgaaly (1993), soil passive pressures from bridge expansion measured behind a 20° skewed integral abutment in Maine indicated substantial skew effects on pressures. The abutment length was 12 m (42 ft). When the greatest expansion occurred, pressures measured 3 m (10 ft) from centerline on the obtuse side of the diaphragm reached levels up to three times higher than the corresponding location on the acute side, and the overall horizontal variation in pressure was greater than the vertical variation. Figure 2-15 and Figure 2-16 illustrate these distributions of horizontal and vertical pressure, respectively. In a similar study on a 15° skew bridge in New Jersey, Khodair (2009) observed similar qualitative behavior in terms of overall pressure distribution.

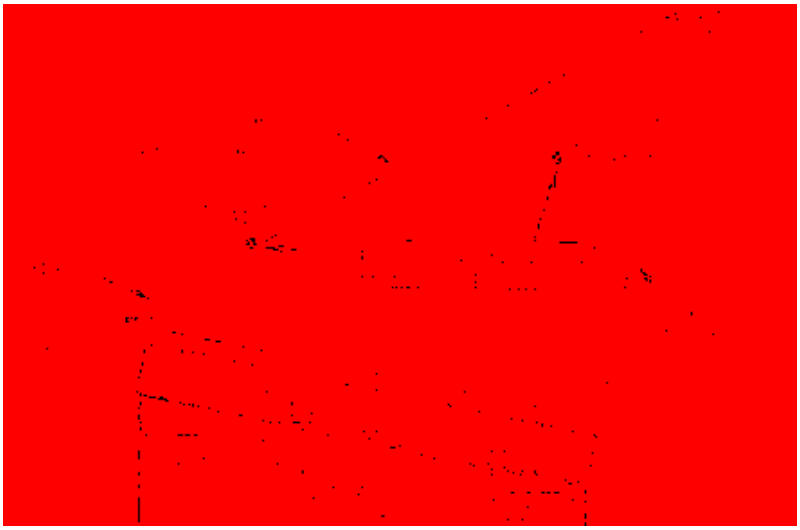

Figure 2-15: Horizontal Passive Pressure Distribution for a Rotating Skewed Bridge (Sandford & Elgaaly, 1993)

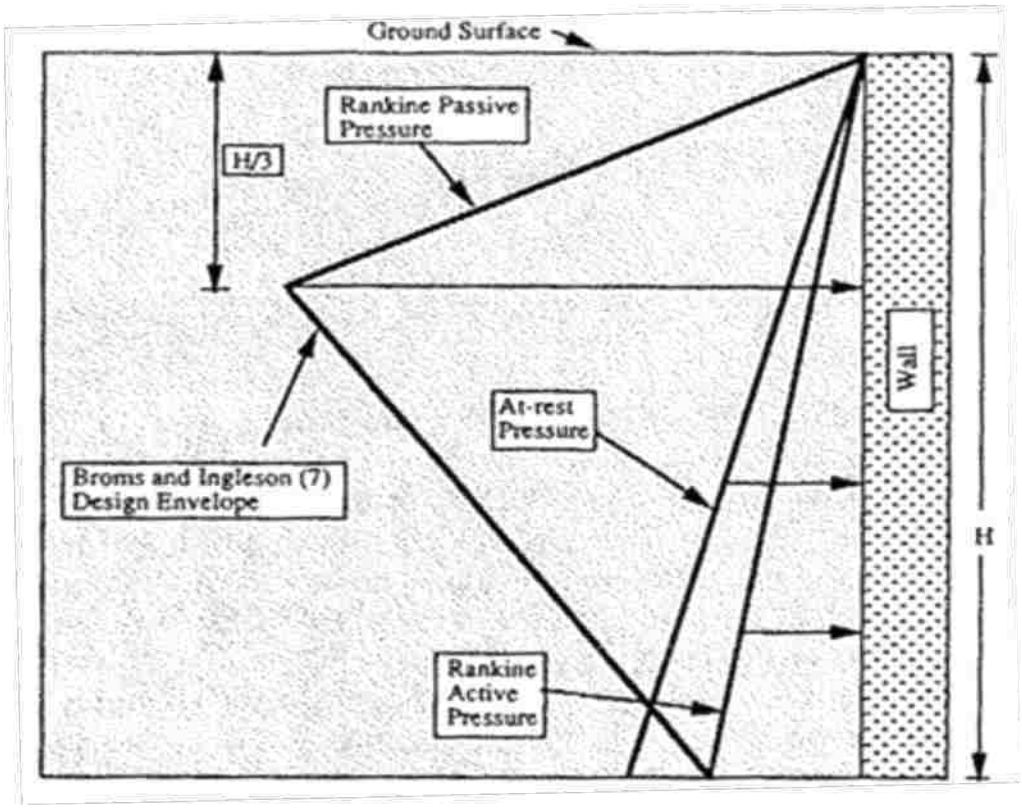

Figure 2-16: Typical Envelope for Lateral Pressures on an Integral Abutment (Sandford & Elgaaly, 1993)

Steinberg and Sargand (2010) observed the forces and movements at the interface of the wingwall and diaphragm of two skewed semi-integral bridges in Ohio. The wingwalls were designed as retaining walls for backfill. However, bridge rotation caused by thermal expansion apparently induced large stresses in the wingwalls, causing cracking as is shown in Figure 2-17.

Numerical analyses performed by Shamsabadi et al., (2006) indicate substantial reduction in passive resistance with increased skew angle. In this particular study, a three-dimensional nonlinear finite element model was developed which estimates soil response behind a skewed abutment during an earthquake. An illustration of the loading simulation is given in Figure 2-18. The model assumes asymmetric loading by the bridge deck as it rotates about the vertical axis. As a result, the obtuse ends of the bridge abutment will apply loading to the backfill soil with

greater intensity and frequency than the acute corners, while the total resistance of the backfill is weakened in comparison to normal abutments. This weakening increases with the skew angle as is illustrated in Figure 2-19, which shows passive force-deflection curves for various skew angles as computed by the model.

Figure 2-17: Cracking, Distress Observed at Ohio Skew Bridge Wingwall (Steinberg & Sargand, 2010)

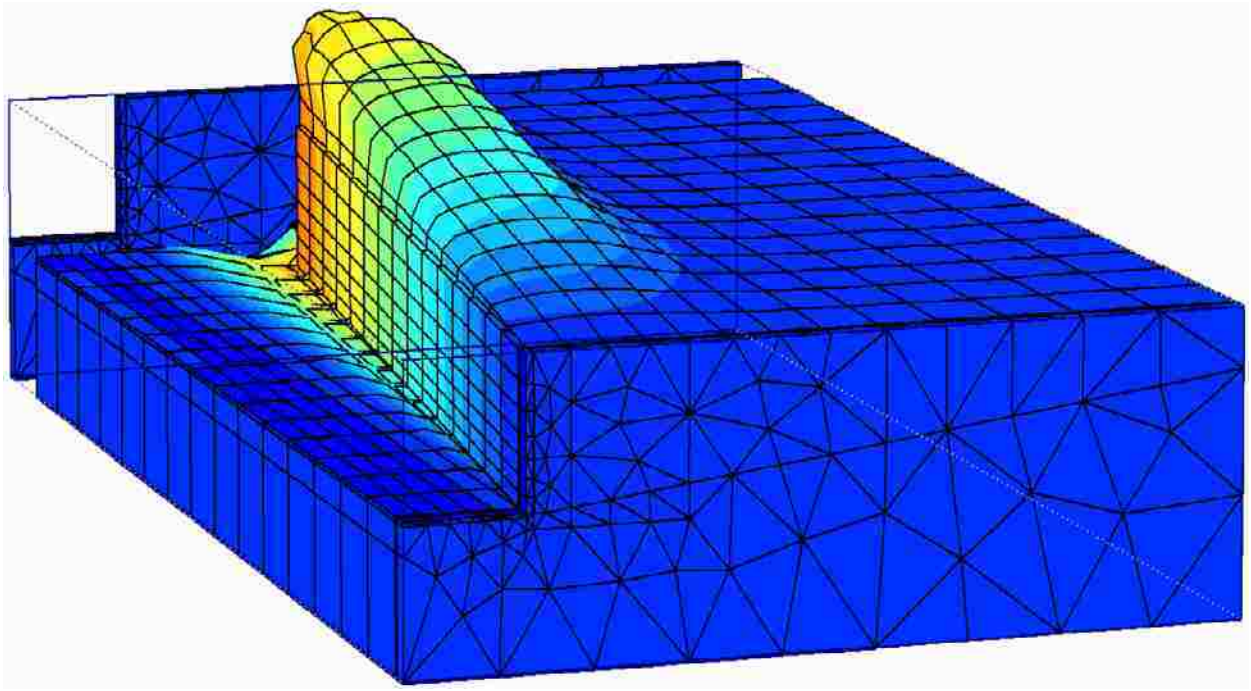

Figure 2-18: Finite Element Model of Backfill Deformation Behind a Rotating 45° Skewed Abutment during Seismic Loading (Shamsabadi et al., 2006)

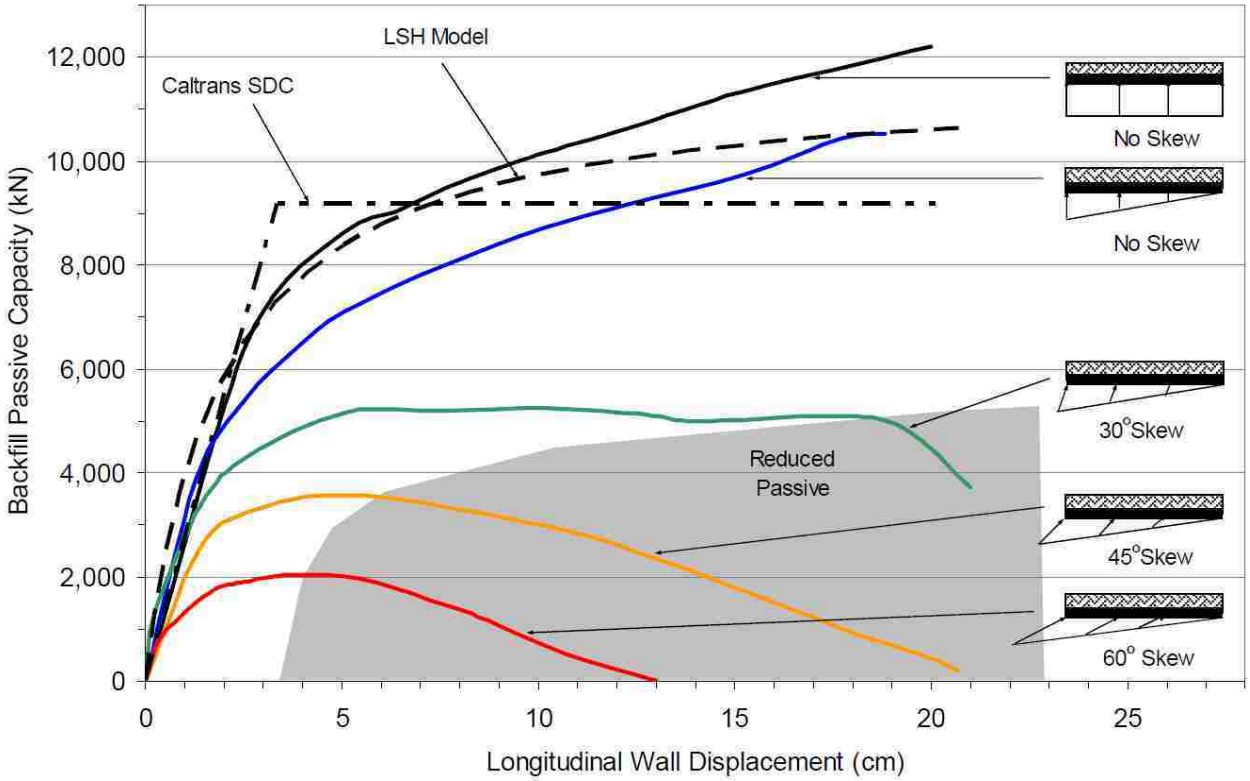

Figure 2-19: Passive Force-Deflection Curves Based on Numerical Modeling (Shamsabadi et al., 2006)

2.6 Limitations of Current Knowledge

Although knowledge gained from performing large-scale passive force tests has been important in developing passive force-deflection curves for bridge abutments, no test results have been available for skewed abutments. Thus, the effect of skew on passive pressure is not well understood. Based on observations discussed in Sections 2.4 and 2.5 of this report, this lack of understanding has important design implications for skewed bridges. With a better understanding of the effect of skew on the passive force-deflection relationship for skewed abutments, the efficiency of skew bridge design could be greatly improved. Such bridges subjected to thermal expansion could be efficiently designed to resist rotation, and damage to wingwalls could be avoided.

In this current study, large-scale tests were performed to determine the effect of skew on the passive-force displacement curve. Since no results for tests of this type have been located in the technical literature, it is presumed that these are the first large-scale tests of this type.

3 LOAD TESTS

3.1 Test Layout

A plan view of the test layout is provided in Figure 3-1. A concrete wall 1.26 m (4.13 ft) wide and 0.61 m (2 ft) high was used to model the backwall of an abutment. Passive force-deflection tests were performed with skew angles (θ) of 0º, 15º, 30º, and 45º. At least two tests were performed for each skew angle to evaluate repeatability. A dense sand was compacted behind the wall to simulate the backfill in a typical approach fill. The sand backfill was 0.9 m (3 ft) thick and extended 0.3 m (1 ft) below the base of the wall to allow a potential failure surface to develop below the wall as might be expected for a Log-Spiral failure geometry. The backfill was 3 to 4 m (10 to 13 ft) long to completely contain the failure surface and was slightly wider than the wall 1.28 m (4.21 ft) to allow the backwall to move into the sand backfill without any friction on the concrete sidewall. To support the sand backfill during compaction, two 1.25 m concrete cubes were bolted to the structural floor of the lab on either side of the fill near the wall. Beyond the concrete cubes, plywood walls were braced into a vertical position. Two plastic sheets were placed along the sidewalls of the backfill to create a low friction surface and produce a 2D or approximately plane strain geometry. A base was constructed below the concrete backwall and rollers were placed at the interface between the bottom of the backwall and the base to provide a normal force but minimize base friction, as is shown in Figure 3-2.

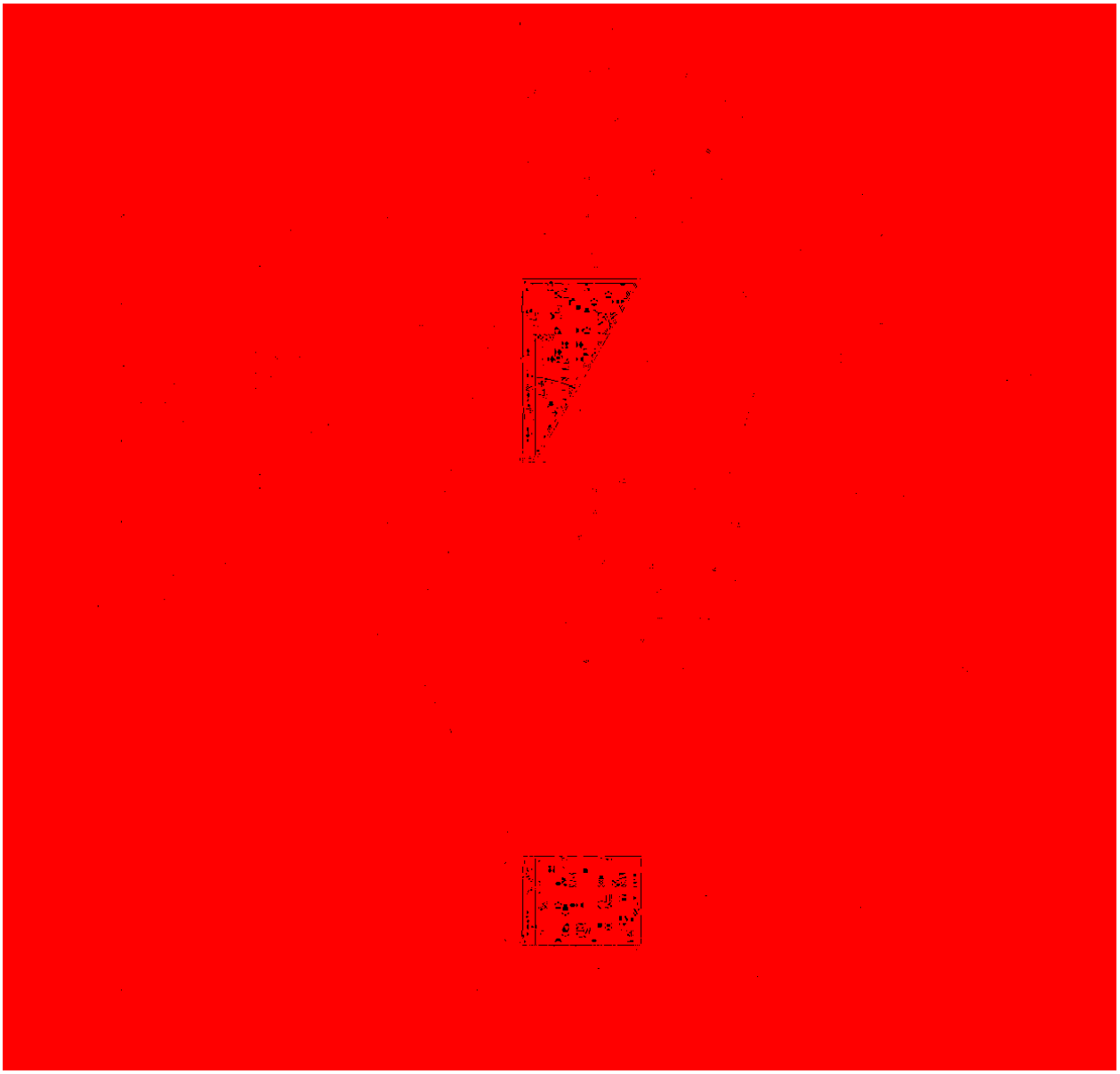

Figure 3-1: Layout for Lab Skew Tests

Tests were performed by pushing the backwall longitudinally into the backfill sand using a 490 kN (110 kip) hydraulic actuator which was bolted to the backwall. The tests were performed with a displacement-controlled approach and the actuator moved into the backfill at a rate of 0.25 mm/min (0.1 inch/min). Vertical and horizontal load cells were mounted between the reaction frame and the actuator so that the loads necessary to hold the wall in place could be

measured directly. Nevertheless, because of the flexibility of the actuator piston, there was still a small amount of movement of the backwall at the soil-wall interface.

Figure 3-2: Photographs Taken During Placement of 45° Backwall

3.2 Instrumentation

Longitudinal load was measured by pressure transducers in the actuator. To measure the movement of the backwall, four longitudinal string potentiometers were positioned at the corners of the wall and two transverse string pots were positioned at the top and bottom of one side. In addition, a final string pot was used to monitor the vertical movement. Longitudinal string pots were also attached to steel rods driven into the backfill surface at distances of approximately 0.6, 1.2, and 1.8 m (2, 4 and 6 ft) behind the backwall to determine average compressive strain within the backfill soil.

To help identify the position of the failure surface on the ground, 0.3 m square grids were marked on the surface of the backfill. The change in elevation of the centerline of the backfill

was also measured at each grid point with a survey level. To locate the failure surface within the backfill, a hand auger was used to drill 50 mm (2 inch) diameter vertical holes through the backfill at a series of locations along the centerline behind the backwall. These holes were then backfilled and compacted with red sand. At the conclusion of each test, a longitudinal trench was excavated and the offset in the red sand column provided the location of the failure surface with distance from the wall face.

3.3 Geotechnical Properties of the Backfill

A summary of the geotechnical properties of the backfill is provided in Table 3-1. In computing the void ratio *e*, it was assumed that the specific gravity G_s of the soil is 2.65. All other properties listed are based on actual measurements. The sand backfill is clean poorly-graded sand classifying as SP according to the Unified Soil Classification System and A-1-b according to the AASHTO system. The particle size distribution curve falls within the gradation limits for washed concrete sand (ASTM C33) as shown in Figure 3-3 with C_u of 3.7 and C_c of 0.7.

3.3.1 Backfill Unit Weight and Moisture Content

A modified Proctor test was performed on the sand and indicated a maximum dry unit weight of 115.4 pcf with an optimum moisture content of 16%. A plot showing dry unit weight versus moisture content is provided in Figure 3-4. The sand was compacted into the box with a jumping jack type compactor in 150 mm (6 inch) lifts to achieve an average relative compaction greater than 95% as specified by many design standards. Relative compaction was measured primarily using a nuclear gauge, with some tests taken using the Sand Cone Method in order to verify accuracy.

Table 3-1: Geotechnical Properties of Backfill Soil

Property	Value
USCS Classification	"SP"
Coefficient of Uniformity, C_u	3.7
Coefficient of Curvature, C_c	0.7
Specific Gravity, G_s	2.65
Void Ratio, e	0.49
Friction Angle, ϕ (°)	46
Wall Friction Angle, δ (°)	33.2
Modified Proctor $\gamma_{d(max)}$	115.4
Optimum Water Content, w_{opt}	16.0
Dry Unit Weight, γ_d	111.0
Relative Density, D_R *(%)*	80
w_{avg} (%) (during compaction)	11.3
w_{avg} (%) (during testing)	8.0
Degree of Saturation, S_{avg} (%)	43
Matric Suction, ψ_{avg} (kPa)	9.7
Apparent Cohesion, $c_{a(avg)}$ (kPa)	3.8

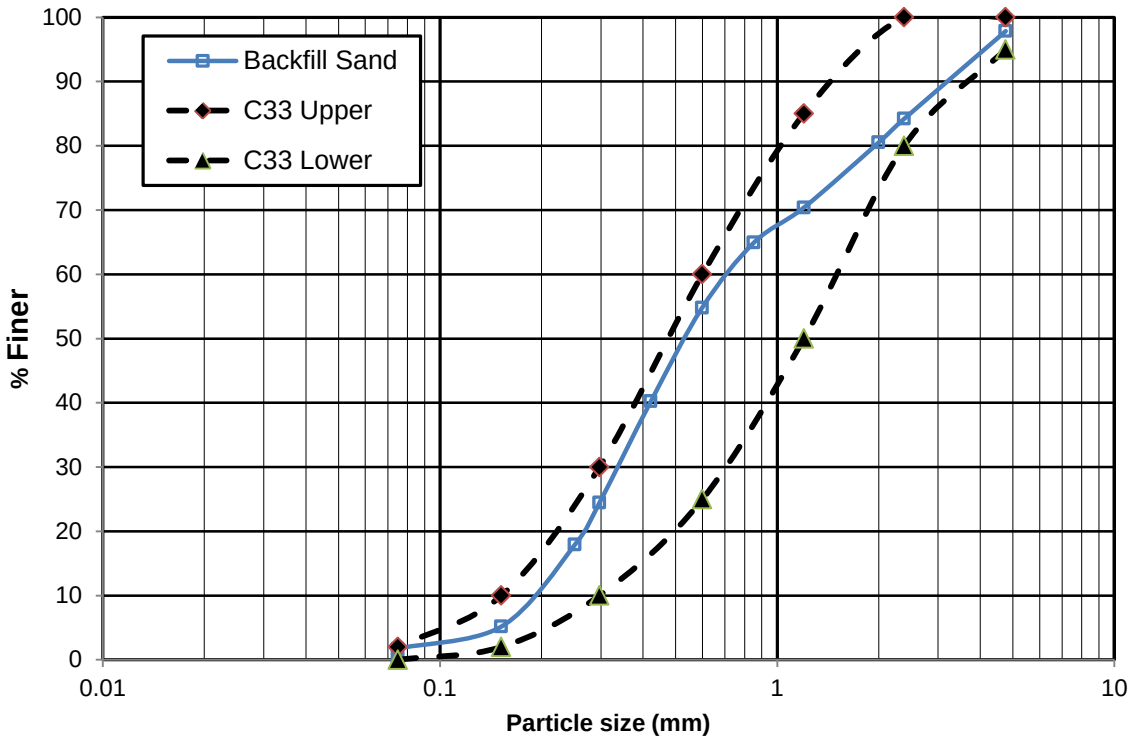

Figure 3-3: Particle Size Distribution for Backfill Sand

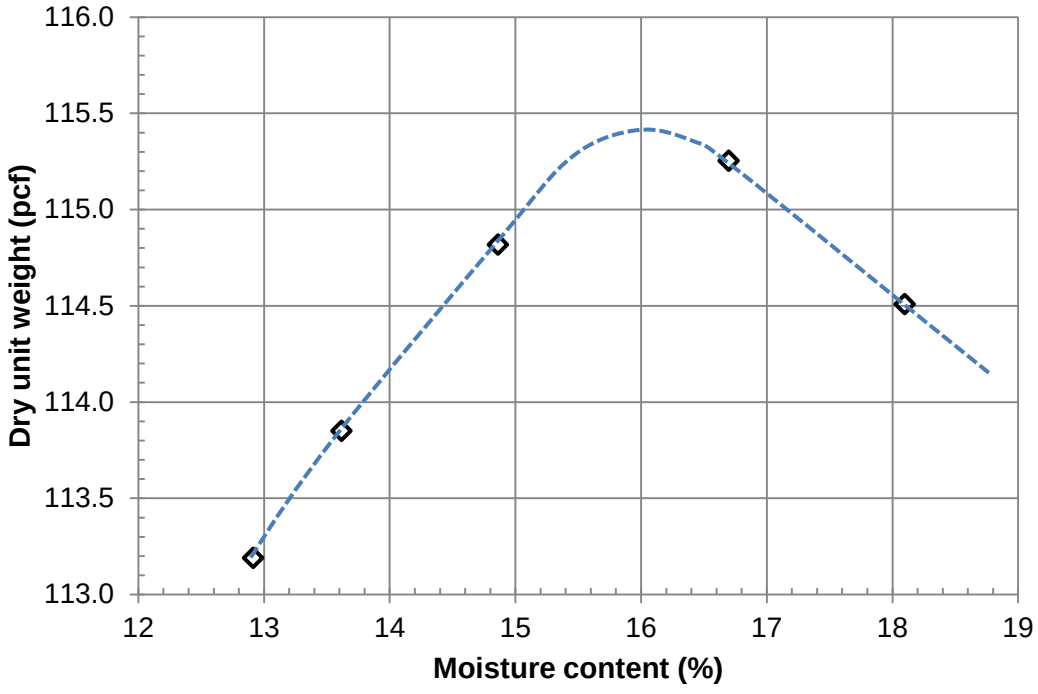

Figure 3-4: Plot of Dry Unit Weight versus Moisture Content According to ASTM D1557

A summary of the mean and standard deviations of the relative compaction for each test is provided in Table 3-2. Histograms of relative compaction based on nuclear density test results for the various skew angles are provided in Figures 3-5, 3-6, 3-7, and 3-8. The average relative compaction overall was 96.5% with a moisture content of 8.0%. Testing was generally performed two days after compaction and moisture content samples were taken immediately after testing. A plot of moisture content versus depth for the various tests is provided in Figure 3-9. The moisture content curves for the various tests generally fall within a one or two percent of one another indicating good consistency between tests.

Table 3-2: Backfill Relative Compaction for Each Test

	Relative Compaction (%)								
	0° Skew			15° skew		30° skew		45° skew	
	Test 1	Test 2	Test 3	Test 1	Test 2	Test 1	Test 2	Test 1	Test 2
	96.9	97.7	95.6	97.1	97.5	95.8	96.8	94.6	96.3
	97.6	96.8	95.1	95.8	96.4	94.6	96.5	97.7	95.8
	96.3	98.4	96.6	94.9	96.5	98.0	96.8	95.6	94.3
	98.0	96.7	96.8	96.7	95.1	95.6	95.7	95.1	94.4
	96.4	97.9	93.8	97.0	98.3	95.8	97.1	95.1	96.6
	97.5	97.7	94.8	94.1	95.1			95.1	94.1
	97.3	98.6	97.7					95.5	97.1
	96.4	96.7	95.8					95.4	96.7
	97.6	98.0	95.5						
	97.9	95.8	94.5						
	95.6	97.7	93.3						
		95.3	95.1						
mean:	97.0	97.3	95.4	95.7	96.3	96.4	96.5	95.3	95.7
st. dev.	0.8	1.1	1.4	1.4	1.5	1.4	0.8	0.2	1.4

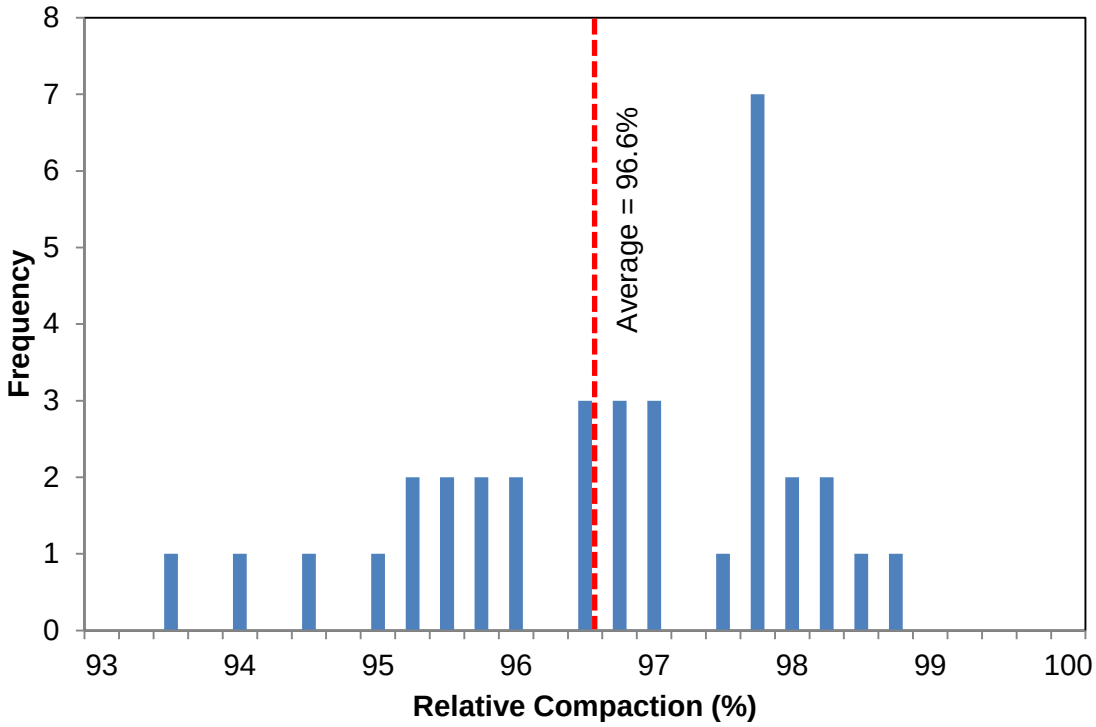

Figure 3-5: Relative Compaction Histogram for Non-Skew Tests

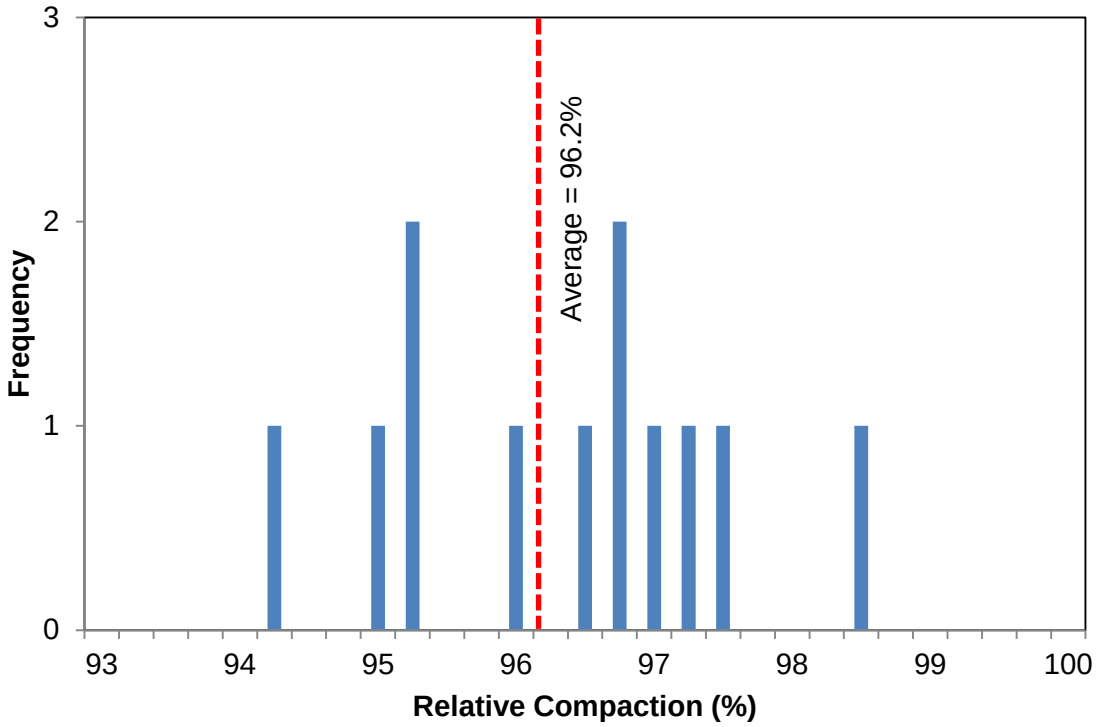

Figure 3-6: Relative Compaction Histogram for 15° Skew Tests

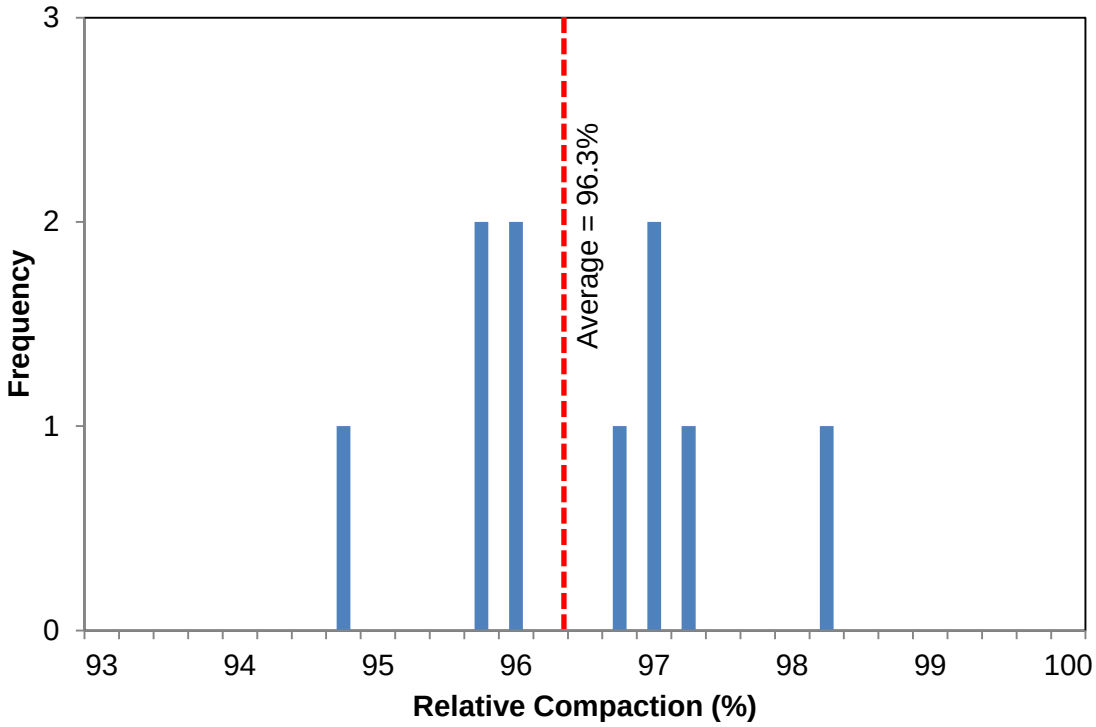

Figure 3-7: Relative Compaction Histogram for 30° Skew Tests

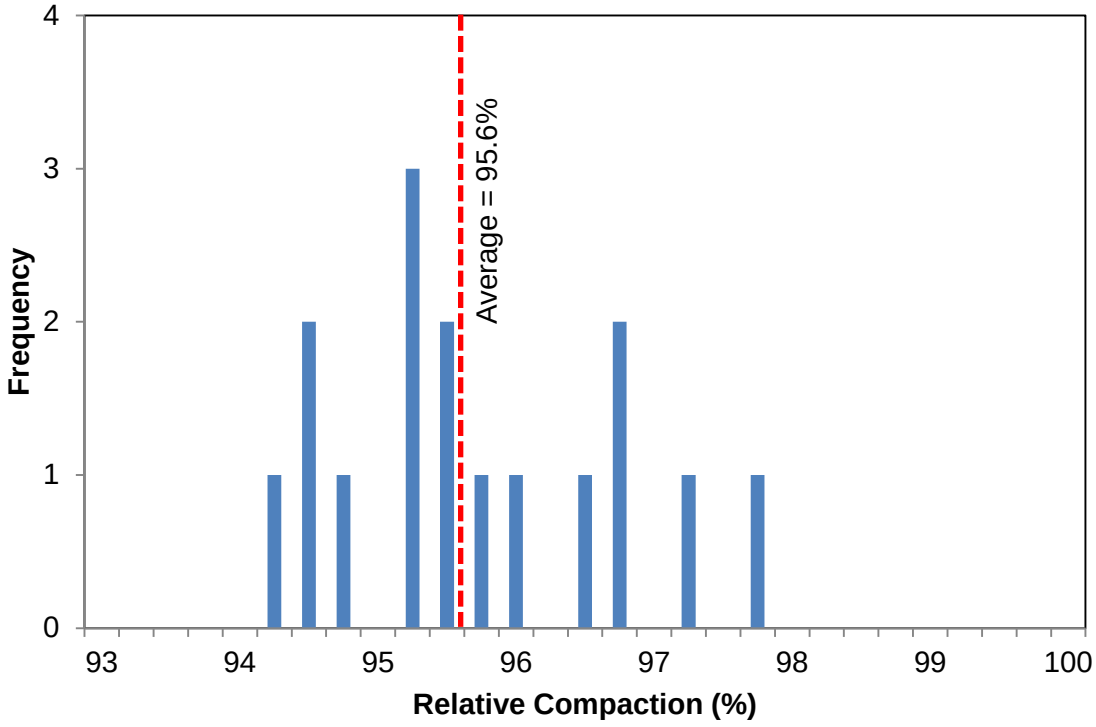

Figure 3-8: Relative Compaction Histogram for 45° Skew Tests

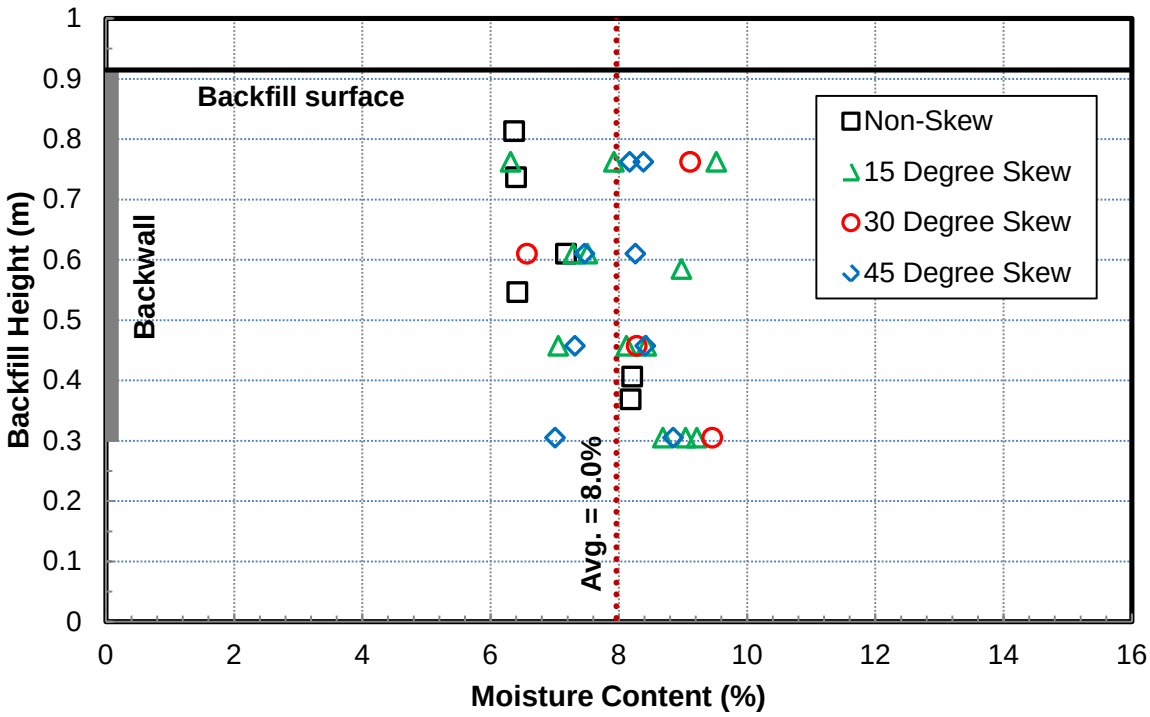

Figure 3-9: Backfill Moisture Content versus Height for the Various Tests

3.3.2 Backfill Shear strength

Based on a direct shear test on the moist sand, the drained friction angle ϕ' was found to be 46º with an apparent cohesion of 4 kPa (80 psf). Interface friction tests were also performed between the sand and the concrete and a wall friction angle δ of 33º was measured. Therefore, the δ/ϕ is 0.72 which is in good agreement with results from other researchers (Potyondy, 1961; Rollins & Cole, 2006). Graphical results from the direct shear test and from the interface friction test are provided in Figures 3-10 and 3-11, respectively.

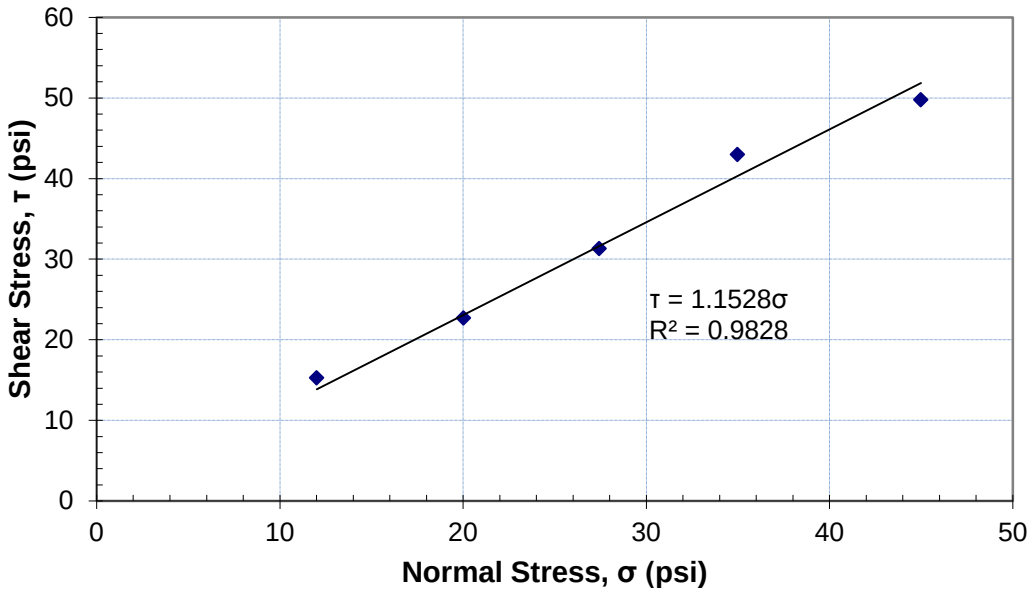

Figure 3-10: Direct Shear Test Results for Backfill Sand

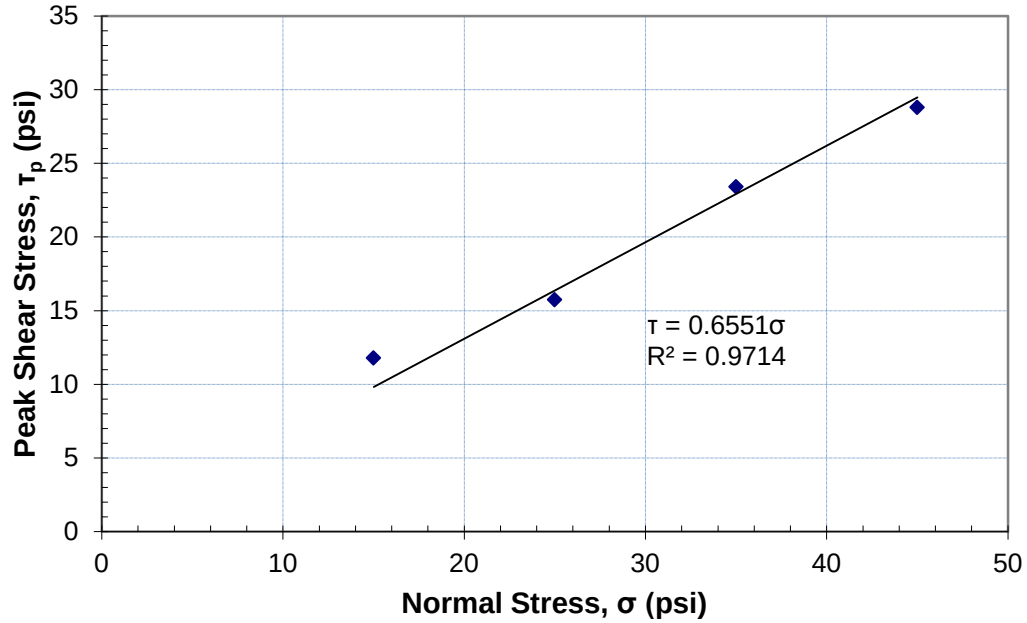

Figure 3-11: Soil-Wall Interface Friction Test Results

Because the compacted sand in a partially saturated state could be excavated with a vertical face and remained stable for long periods, the potential for apparent cohesion owing to

suction was also investigated. A plot of matric suction versus degree of saturation is provided in Figure 3-12 based on testing conducted at the BYU Soil Physics Lab. Based on these lab results, the matric suction ψ can be estimated using Equation 3-1.

$$\psi = 1.582\ S^{-2.152} \tag{3-1}$$

where ψ is in units of kPa and S is the degree of saturation expressed as a fraction. This equation is based on the best fit trend line in Figure 3-12. During the load tests, the average moisture content was 7.96% with a standard deviation of 0.98%. Moisture content was typically (i.e., within one standard deviation from the average) between 7.0 and 8.9%, with a corresponding degree of saturation between 38 and 48%. Based on Equation 3-1, the matric suction for this range was approximately 8 to 13 kPa (150 to 270 psf). A summary of the moisture, degree of saturation, matric suction, and apparent cohesion is provided in Table 3-3. The moisture characteristic curve for the backfill material, which is a plot of the best fit trend in Figure 3-12 on an arithmetic scale, is provided in Figure 3-13.

Based on the recommendations of Likos et al. (2010), the apparent cohesion c_a for a partially saturated sand can be given by the equation

$$c_a = S_e\ \psi \tan \phi' \tag{3-2}$$

where S_e is the effective saturation, equal to $(S - S_r)/(1 - S_r)$ expressed as a fraction and S_r is the residual saturation obtained from the water retention curve. The water retention curve in Figure 3-13 indicates that S_r is about 14%. A plot of apparent cohesion versus degree of saturation

computed using Equation 3-2 is provided in Figure 3-14. The apparent cohesion for the typical range of water content determined from Equation 3-2 was 3 to 4 kPa (about 70 to 90 psf). Analysis according to Log Spiral theory indicates that, for the range of moisture conditions during the testing, apparent cohesion accounts for approximately 26% of the passive resistance of the soil. This cohesion contribution is relatively high because the wall height is relatively small and therefore, the frictional resistance is lower than it would be for a taller abutment wall.

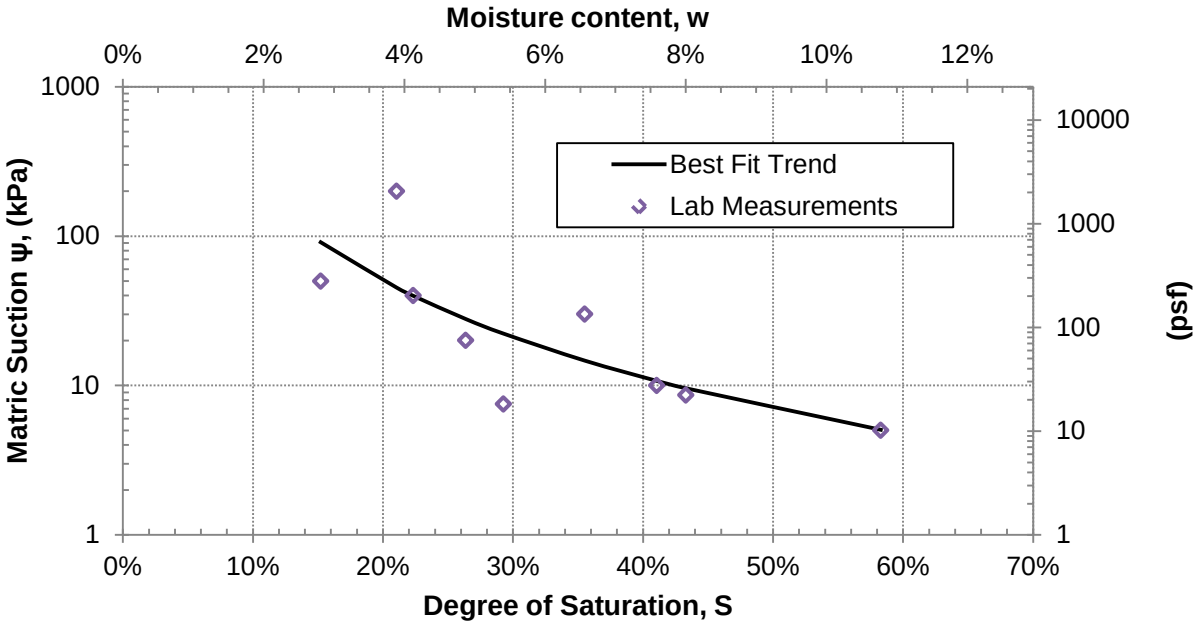

Figure 3-12: Plot of Matric Suction versus Degree of Saturation and Moisture Content

Table 3-3: Summary of Moisture, Degree of Saturation, Suction and Apparent Cohesion Based on Lab Tests

	Moisture Content, *w* (%)	Degree of Saturation, *S* (%)	Effective Saturation, S_e (%)	Matric Suction, *ψ* (kPa)	Apparent Cohesion, c_a (kPa)
Avg.	8.0	43	34	9.7 (200 psf)	3.8 (79 psf)
Standard Deviation	0.98	5.3	6.2	3.2 (66 psf)	0.3 (6.7 psf)
Typ. Range (± 1 st. dev)	7.0-8.9	38-48	28-40	8-13 (160-270 psf)	3.5-4.1 (73-85 psf)

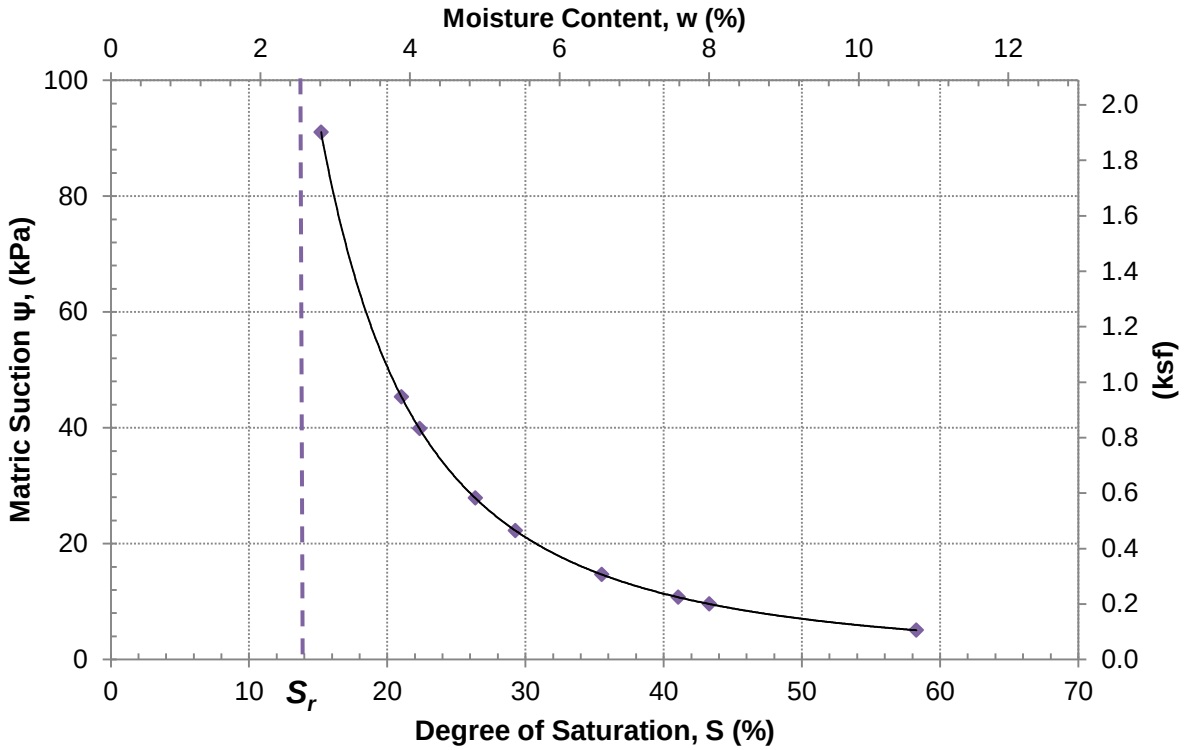

Figure 3-13: Backfill Material Water Retention Curve Based on Best Fit Trend of Lab Measurements

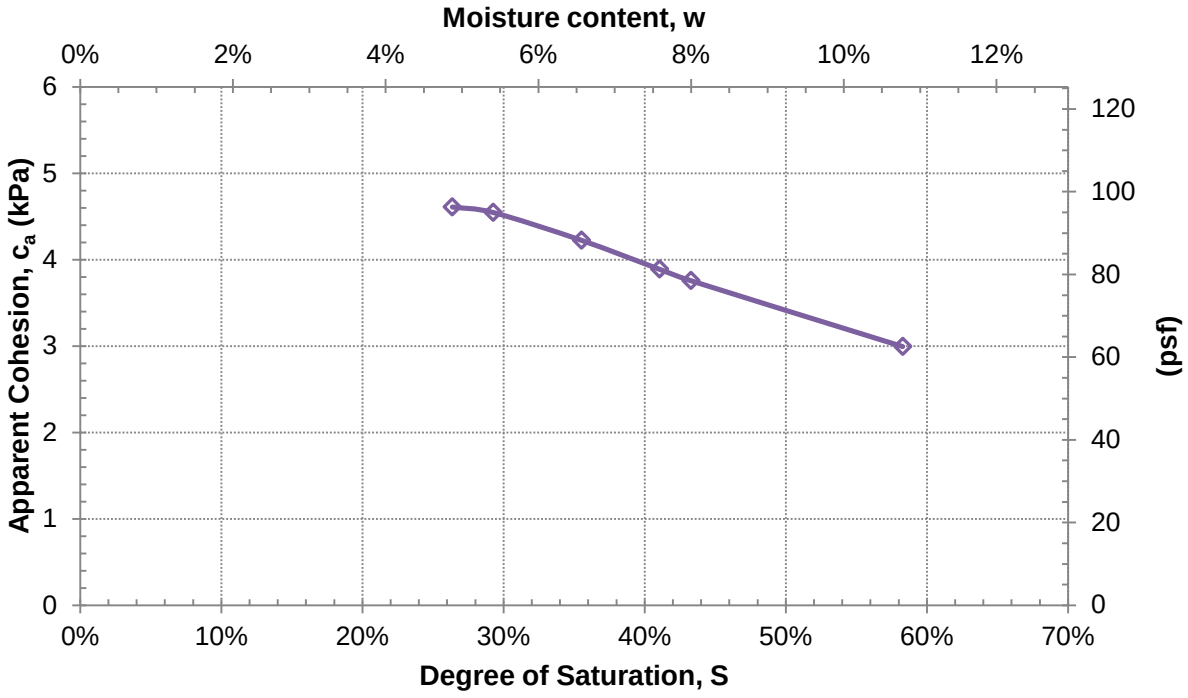

Figure 3-14: Plot of Apparent Cohesion vs. Degree of Saturation and Moisture Content for Typical Conditions During Testing

4 TEST RESULTS

4.1 Passive Force-Deflection Curves

The passive force versus longitudinal deflection curves for the tests at each of the skew angles is plotted in Figure 4-1, and a summary is provided in Table 4-1. The passive force was computed from the applied actuator force (longitudinal force) using Eq. 2-3 while the wall deflection was the average of the four longitudinal strain potentiometers. The passive force and displacement Δ values in Figure 4-1 have been divided by the passive force measured for the no-skew case and the wall height H, respectively, and the resulting normalized passive force-deflection curves are provided in Figure 4-2. The longitudinal force versus longitudinal deflection curves for the tests is plotted in Figure 4-3. Generally, the results from the pair of tests at each skew angle were reasonably consistent; however, some variations are apparent for post-peak response. Although the initial stiffness for each curve is remarkably similar, the peak passive force clearly decreases as the skew angle increases.

While the passive force-deflection curve appears to exhibit a typical hyperbolic curve shape for the no skew case, it transitions to a different shape as the skew angle increases. As the skew angle increases, the passive force exhibits a longer "plateau" where the force remains relatively constant with deflection before abruptly decreasing to a residual value. While this plateau typically increased gradually to a peak, the peak actually occurred at the beginning for some tests.

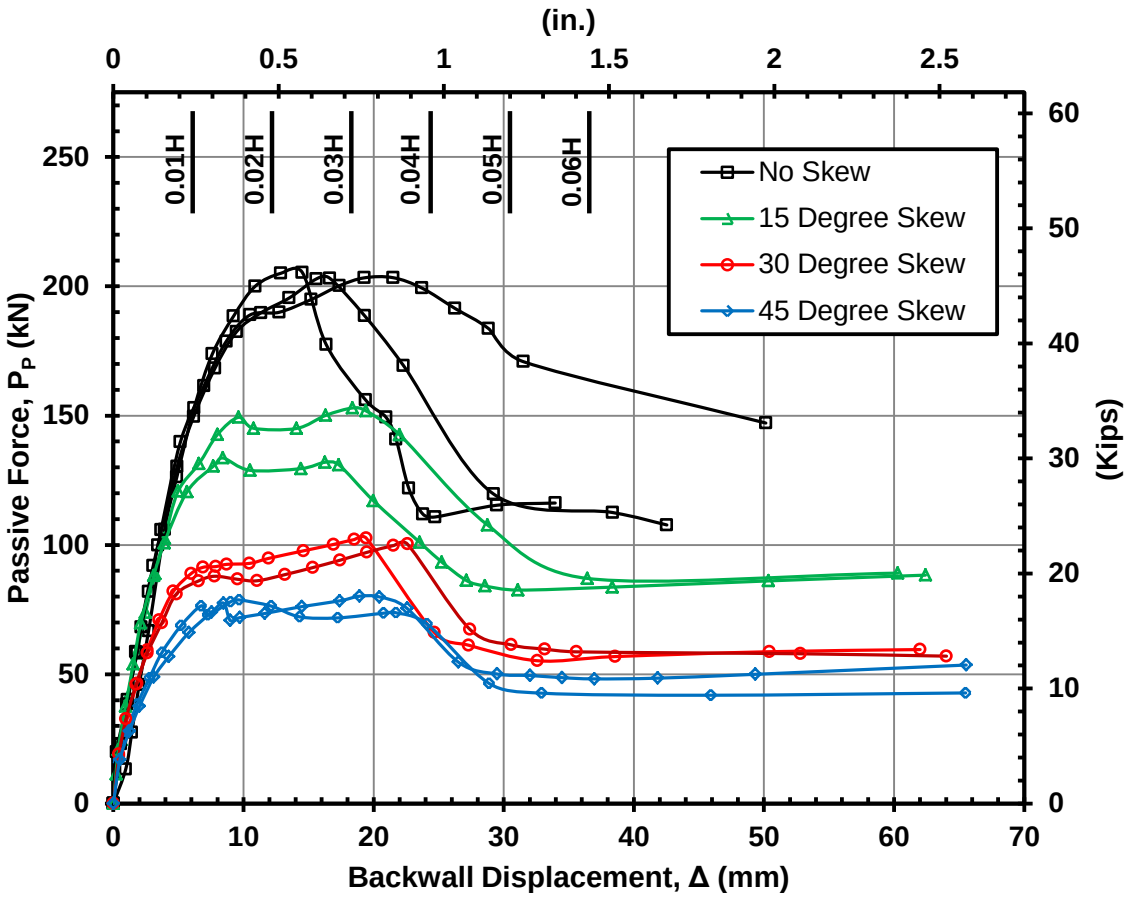

Figure 4-1: Measured Passive Force-Deflection Curves for Various Skew Angles

Table 4-1: Summary of Passive Force Measurements for the Various Skew Angles

Skew	Avg. Passive Force, P_P		P_P (Relative to no-skew case)	Reduction
(°)	(kN)	(Kips)	(%)	(%)
0	204	45.8	100	0
15	146	32.8	72	31
30	117	26.3	57	50
45	112	25.3	55	61

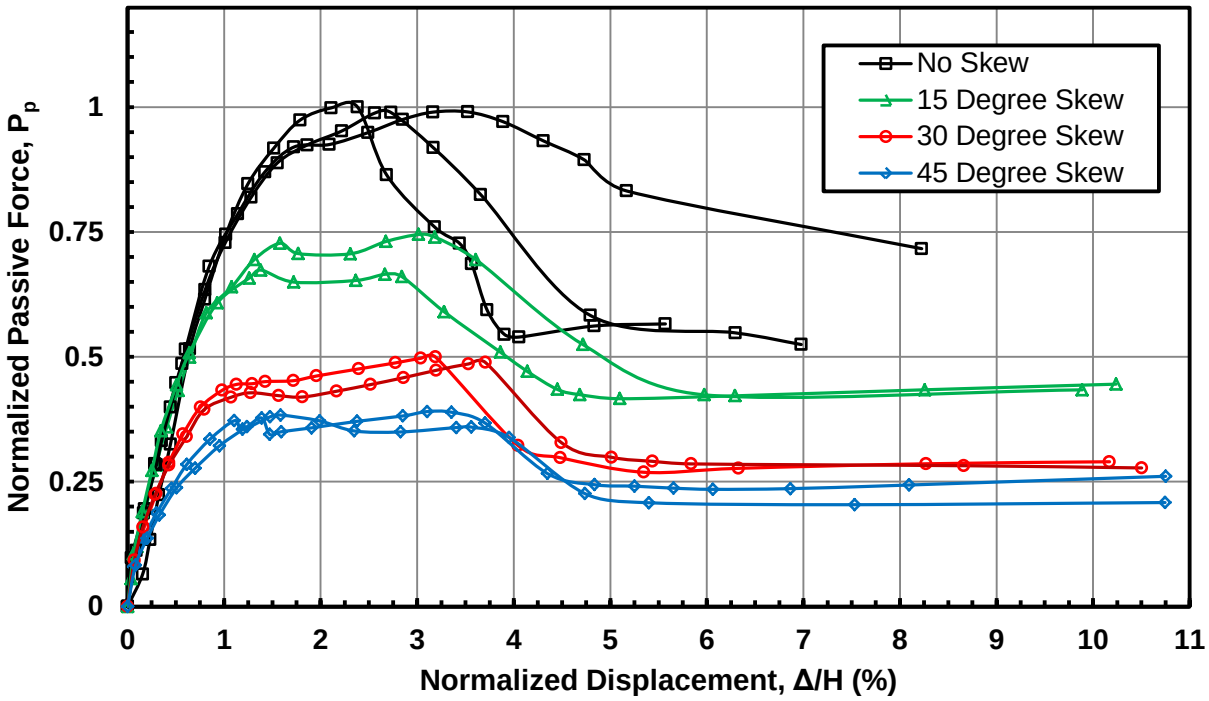

Figure 4-2: Normalized Passive Force-Displacement Curves for the Various Skew Angles

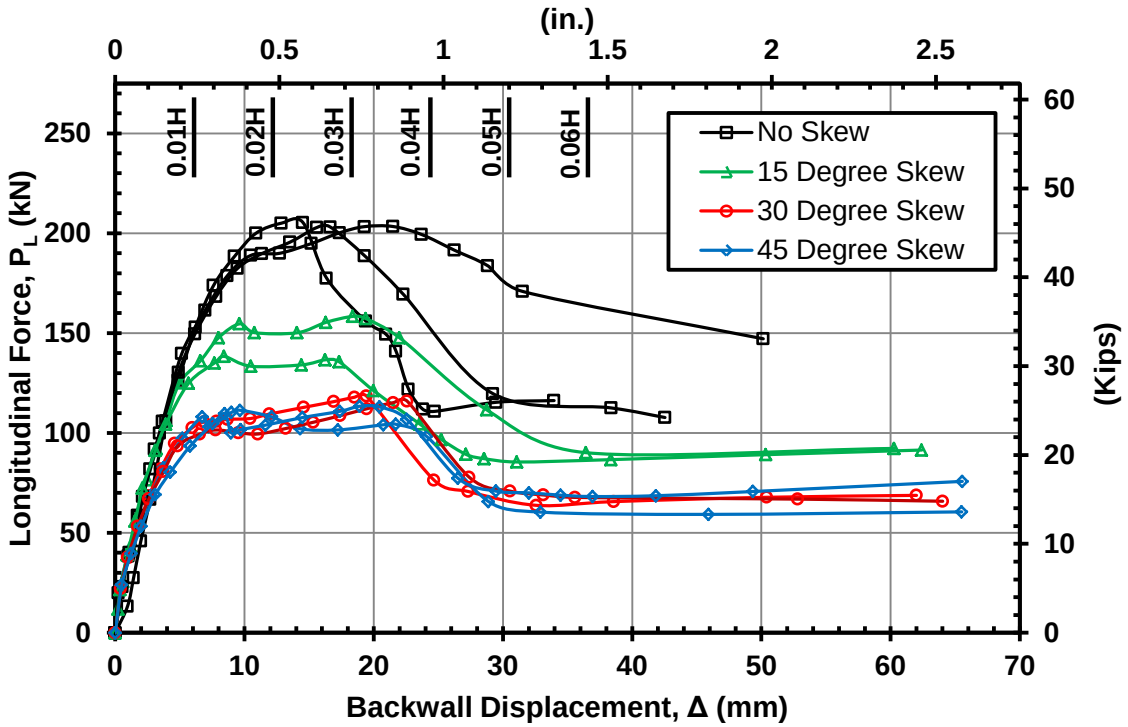

Figure 4-3: Plot of Longitudinal Force versus Displacement for Various Skew Angles

The peak passive force typically developed at a displacement relative to the wall height of 2.5% to 3.5% of the wall height *H*, and did not change consistently with skew angle as is illustrated in Figure 4-4. Test results typically showed a drop off in the passive force to a residual value at a normalized displacement of 0.04*H* to 0.06*H*. This post-peak reduction in passive force to a residual value is consistent with the stress-strain behavior expected from dense compacted sand. Dense sands dilate during shearing and the resulting lower density leads to a reduced strength. The post-peak residual strength values relative to peak strength for the various skew angles are given in Figure 4-5. The post-peak residual strength ranged from 53% to 72% of the peak value with an average of 59%, and may be important for large displacement applications. This drop in resistance is consistent with measurements from the direct shear strength testing wherein residual strength was about 57% of peak strength. The post-peak drop in passive force appeared to become somewhat more abrupt as the skew angle increased.

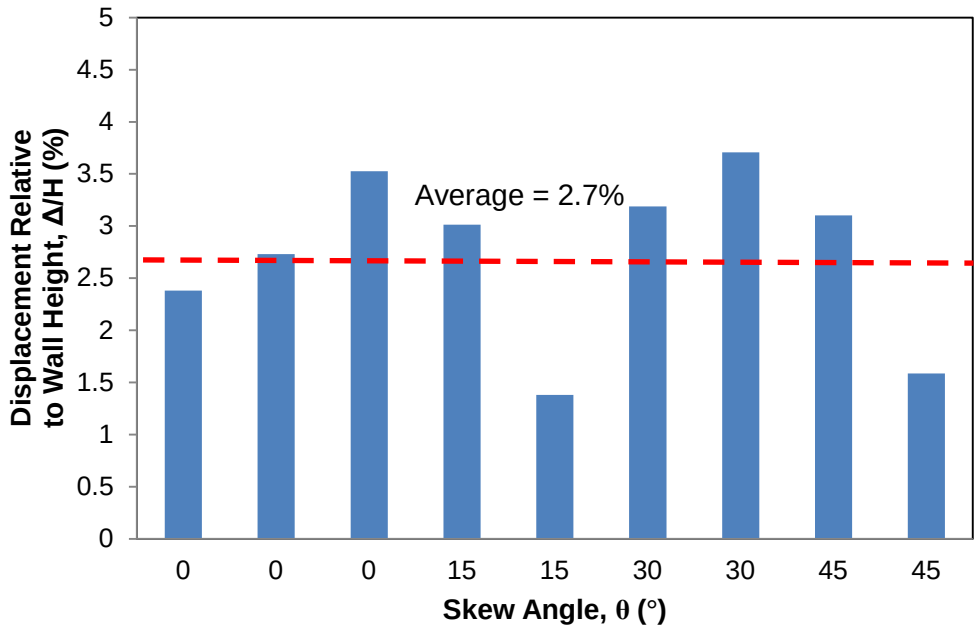

Figure 4-4: Relative Displacement Required for Ultimate Passive Force

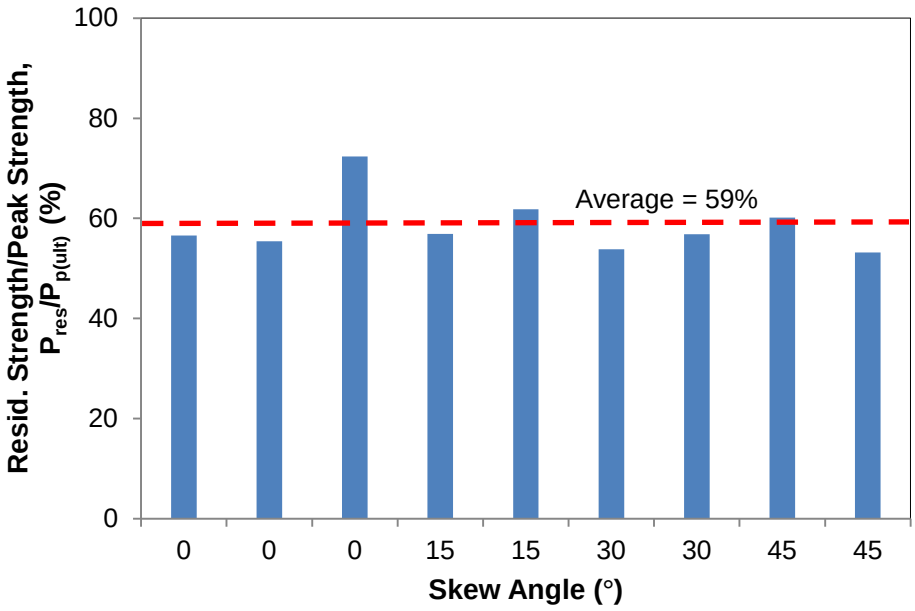

Figure 4-5: Residual Strength Relative to Peak Strength for the Various Skew Angles

The peak passive force from a test at a given skew angle has been divided by the peak passive force at zero skew and is plotted as a function of skew angle in Figure 4-6. As the skew angle increases, the passive force decreases significantly. For example, at a skew angle of 30º the passive force is only about 50% of that with no skew. Similar normalized data from numerical analyses of skew abutments reported by Shamsabadi et al (2006) are also plotted in Figure 4-6 and the results follow the same trend line. The curve has been extrapolated to zero at a skew angle of 90º. As illustrated in Figure 4-7, at a skew angle of 90º there would be no passive force but only transverse shear force equal to the side shear resistance on the wall. There must be a transition [Figure 4-7, part (b)] from pure passive force and zero side shear for 0° skew [Figure 4-7, part (a)] towards pure side shear and zero passive force at 90° skew [Figure 4-7, part (c)]. Of course, the side shear resistance at 90° skew would be much less than the passive force at 0° skew. The agreement between the numerical and physical test results suggests the potential for a simple adjustment factor to account for skew effects. However, considering that there is a

significant decrease in capacity, these large-scale results should be verified with full-scale field tests with variations in abutment geometry and possibly backfill type.

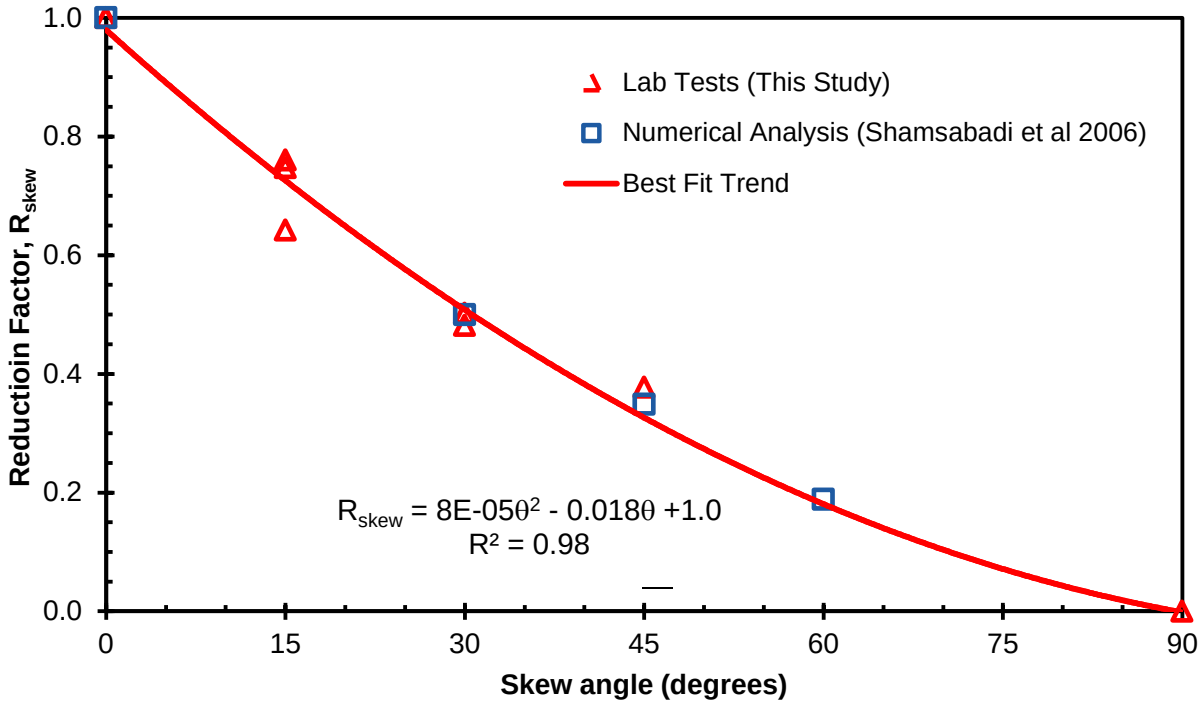

Figure 4-6: Reduction Factor, R_{skew}, Plotted versus Skew Angle Based on Test Results and Numerical Analyses

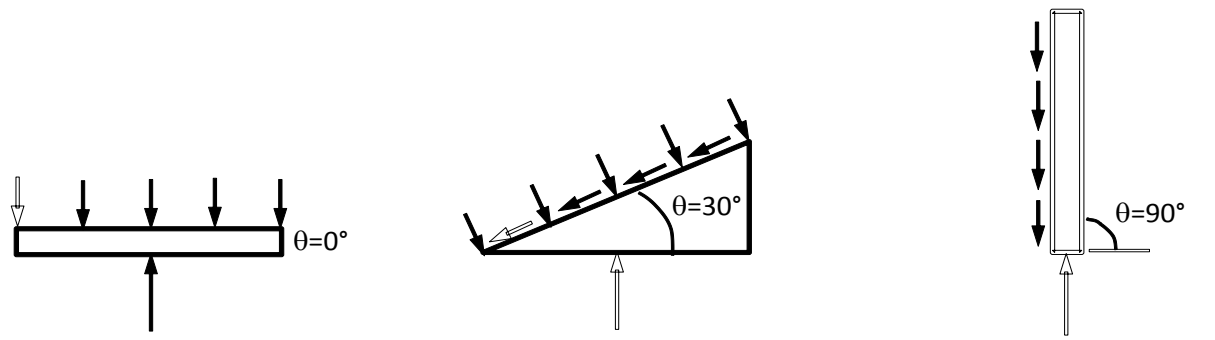

(a) θ = 0°
Pure Passive Resistance,
No Shear Resistance

(b) 0° < θ < 90°
Combined Passive Resistance
and Shear Resistance

(c) θ = 90°
Pure Shear Resistance,
No Passive Resistance

Figure 4-7: Illustration of Transition of Resistance on Back Wall from Pure Passive Resistance at 0° Skew to Much Lower Side Shear at 90° Skew

4.2 Backwall Movement

As indicated previously, vertical and lateral displacement of the wall was measured during each test and the maximum values are summarized in Table 4-2. These displacements are also given graphically in Figures 4-8 and 4-9. A review of the data in Table 4-2 indicates that displacement was less than 4.4 mm for vertical movement and less than 2.3 mm for transverse movement for the skew angles tested.

Table 4-2: Backwall Maximum Vertical and Transverse Movements

Backwall Movement (mm)		
Test	Vertical Disp.	Transverse Disp.
No Skew	1.5	-
No Skew	2.0	-
15°	3.4	1.3
15°	4.4	1.4
30°	0.02	2.1
30°	2.0	2.3
45°	1.4	1.8
45°	1.3	1.8
max:	**4.4**	**2.3**

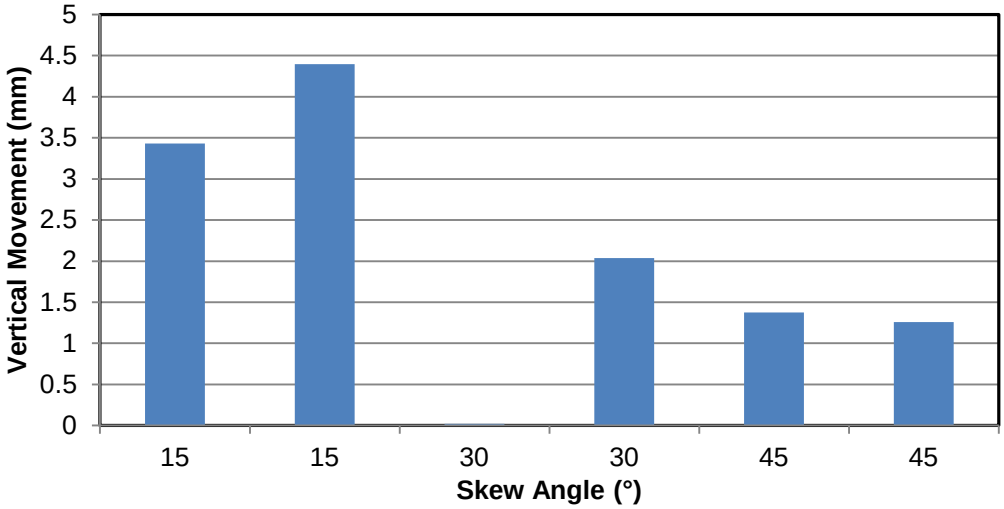

Figure 4-8: Vertical Movement of Backwall for the Various Tests

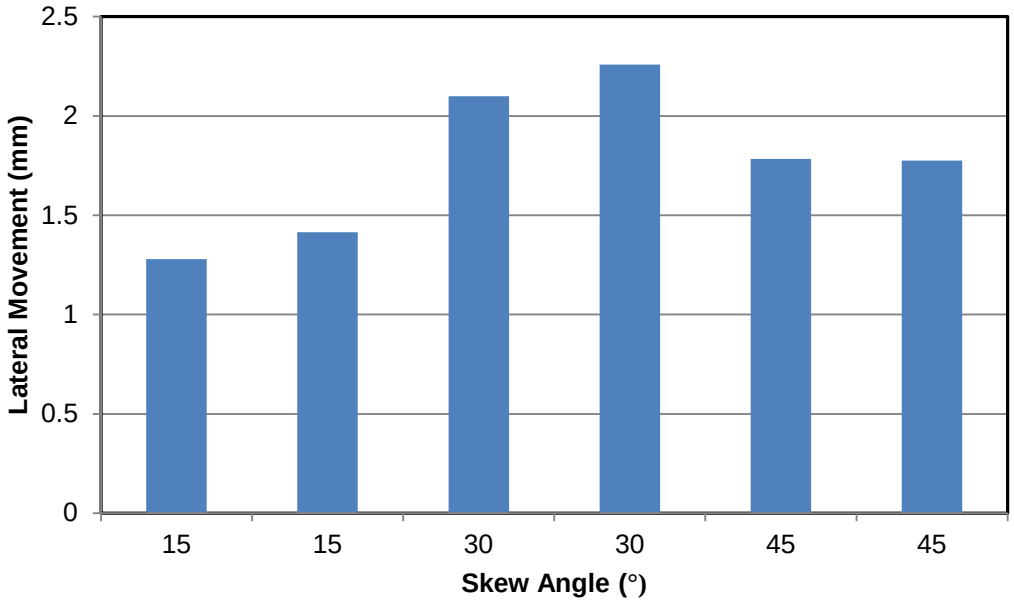

Figure 4-9: Transverse Movement of the Backwall for the Various Skew Tests

Despite the rigidity of the loading system, longitudinal movements at the four locations on the wall indicated slight differential movement between the top and bottom of the wall. The average differential movement was 0.4% (greater movement at the bottom of the wall), with 0.7% being the greatest magnitude of differential movement. These movements correspond to relative wall rotations about the transverse axis of 0.2° and 0.4°, respectively.

4.3 Variation of Forces with Skew Angle

The peak longitudinal force P_L, peak passive force P_P, peak transverse shear force P_T (computed using Eq. 2-4), and the peak transverse shear resistance P_R (computed using Eq. 2-5) are plotted versus skew angle in Figure 4-10. In computing P_R, the wall friction was taken as 33° with apparent cohesion of 4 kPa (80 psf) based on the lab test results. Although the passive force continues to decrease with skew angle, as explained previously, the longitudinal force appears to

stabilize somewhat at a skew angle of 30°. Apparently, the decrease in passive resistance is partially compensated by the increased longitudinal component of the shear resistance.

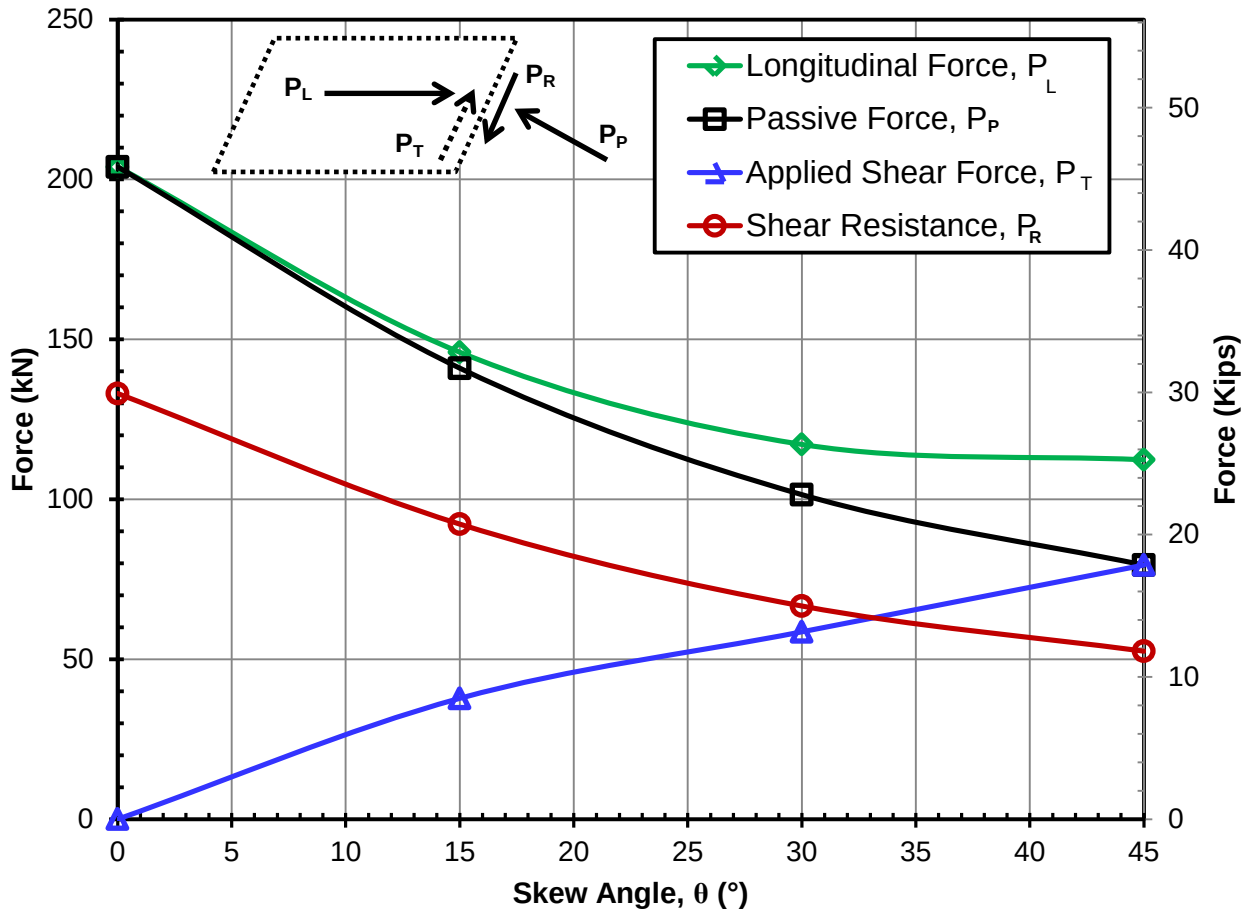

Figure 4-10: Plot of Longitudinal Force P_L, Passive Force P_P, Transverse Shear Resistance P_R and Applied Shear Force P_T as a Function of Skew Angle

While the applied shear force increases with skew angle, the shear resistance decreases because the normal force provided by the passive force decreases. Nevertheless, as shown in Figure 4-10, the lateral shear resistance is greater than the applied lateral shear force in all cases except for the 45° skew. This explains the lack of significant lateral displacement for measured lateral force for these cases. For the 45° skew case, the transverse shear resistance is lower than

the transverse shear force and greater transverse force was measured by the load cell. The measured side load (perpendicular to longitudinal load) corresponding to the peak passive force for each test is is provided in Figure 4-12. The steady increase in measured side load suggests that wall friction mobilized incrementally with increasing skew angle, and that full mobilization of wall friction occurred between skew angles of 30° and 45°. This is consistent with the intersection of the applied shear force and shear resistance in Figure 4-11.

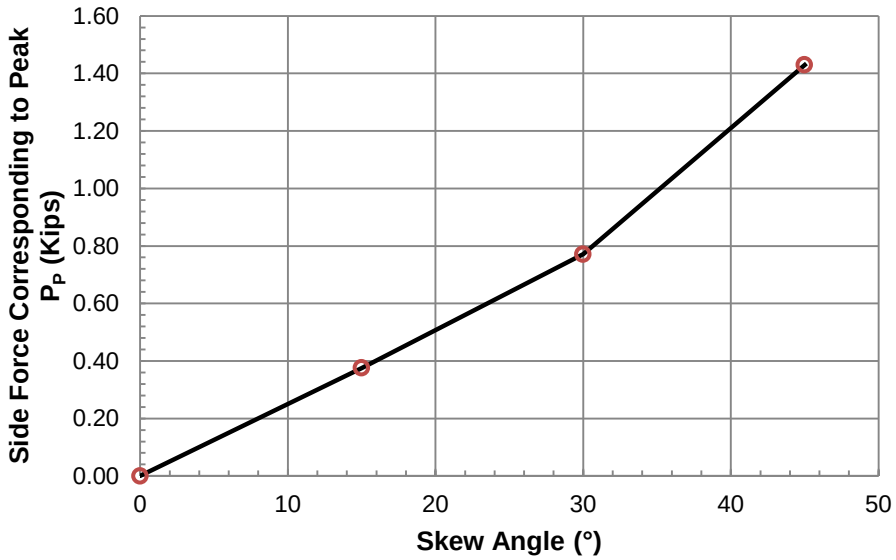

Figure 4-11: Plot of Side Load Corresponding to Peak Passive Pressure vs. Skew angle

4.4 Failure Surface Geometry

The failure surface for the no skew case was about the same length across the width of the sand box; however, when a skew angle was involved, the failure surface also exhibited a skew across the width of the sand box. The photos in Figures 4-12 and 4-13 show the failure surface geometry at the ground surface for one of the non-skew tests and one of the 30° skew tests, respectively. The failure surface did not manifest itself at the ground surface until after the

peak force had been reached and the passive resistance had begun decreasing to the residual value.

The failure surface within the sand was clearly identifiable from the offset in the red sand columns as shown by the photo in Figure 4-14. For columns closer to the wall, there was typically a lower shear offset in the column with a bent section above it and then another shear offset above the bent section. In contrast, for columns further away from the wall and closer to the ground surface there was simply one shear offset in the column. This failure pattern suggests that the soil near the wall may be compressing more than soil away from the wall in addition to shearing along the failure surface.

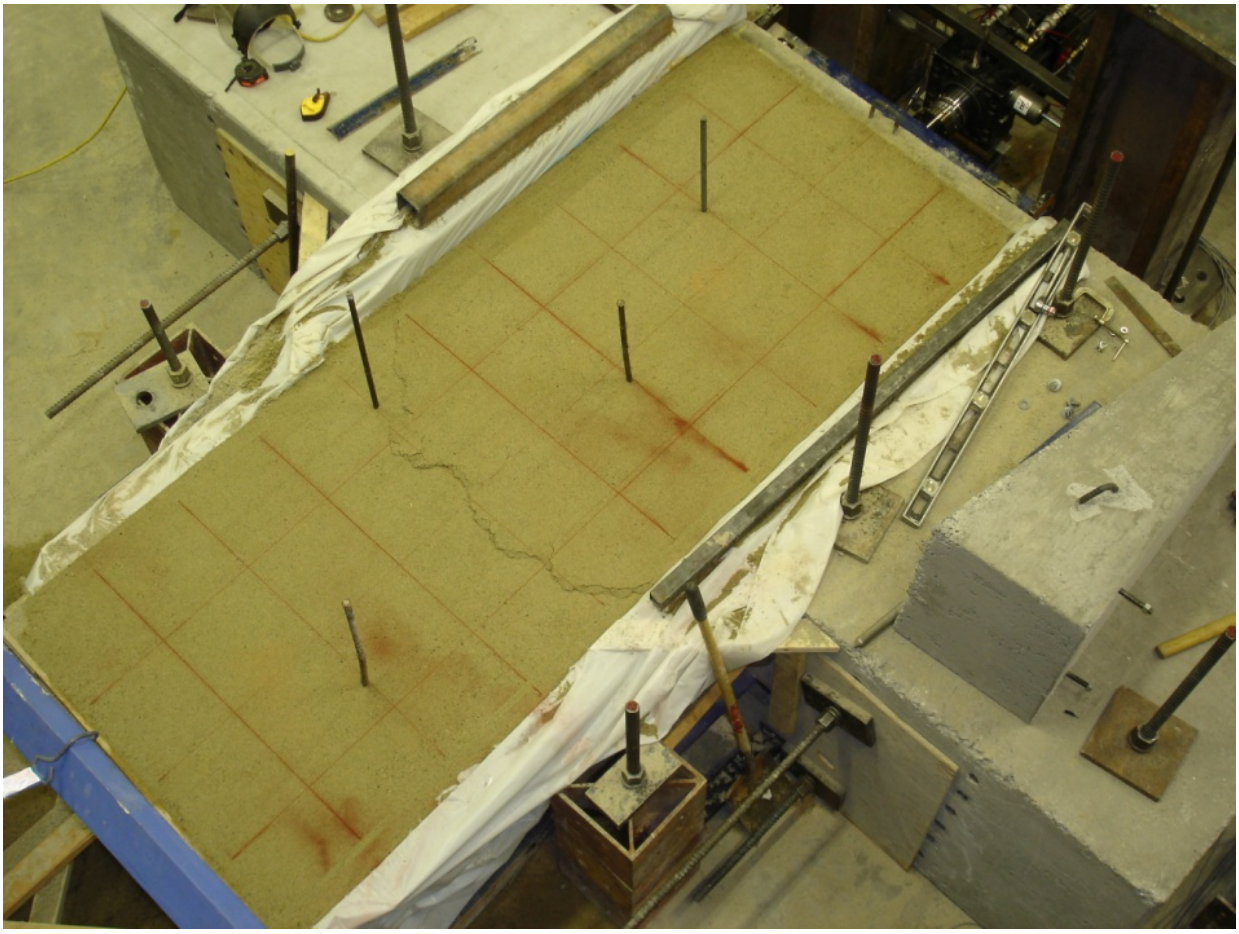

Figure 4-12: Photograph Showing Failure Surface Geometry at Ground Surface for Non-Skew Test

Figure 4-13: Photograph Showing Failure Surface Geometry at Ground Surface for 30° Skew Test

Figure 4-14: Photographs Showing Failure Surface Geometry Within Sand Based on Offset in Red Sand Columns for 45° Skew Test

The failure surface geometry is plotted as a function of distance behind the middle of the wall for the various skew angles in Fig. 4-15. In addition, the ground surface heave is also plotted for each test. The average length of the failure surface behind the middle of the wall was 2.1 m (7.0 ft) with a standard deviation of 0.3 m (1.0 ft). The length of the failure surface ranged from 1.8 to 2.6 m (5.9 to 8.6 ft). The failure surface typically extended 75 mm to 300 mm (3 to 12 inch) horizontally from the bottom of the wall then exhibited a relatively linear trend line upward to the surface. The angle of inclination of the trend line was between 19º and 21.5º with an average of 20°. Because the angle of inclination of the failure wedge α is given by the equation

$$\alpha = 45 - \phi'/2 \qquad (4\text{-}1)$$

according to many failure theories, the interpreted drained friction angle would be between 47º and 52º with an average of 50º. This inferred friction angle is higher than the measured friction angle from the direct shear test, but is close to what would be expected for the plane strain friction angle. Based on a number of studies, Kulhawy and Mayne (1990) found that the plane strain friction angle for dense sand was 11% higher than the triaxial value on average. This would indicate that the plane strain friction angle for this sand would be about 51°, which is very close to the inferred angle from the tests. Of course, the conditions of the box during testing also resemble plane strain geometry.

.

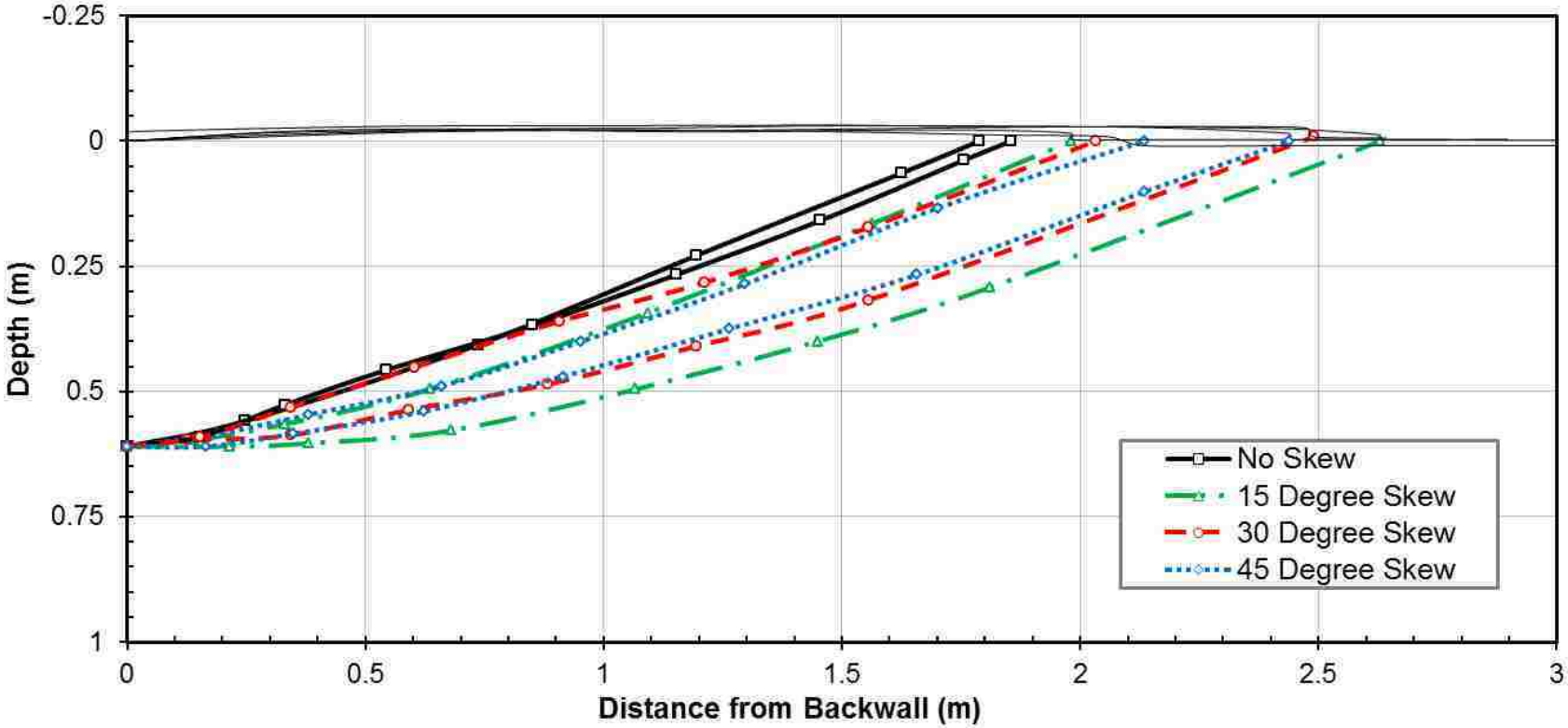

Figure 4-15: Failure Surface Geometry and Ground Surface Heave as a Function of Distance Behind the Wall Along the Centerline for Tests at Various Skew Angles

The heave of the failure wedge was typically about 25 mm (1.0 inch) which represents a 4% heave relative to the maximum thickness of the failure wedge [0.62 m (2 ft)]. The heave was relatively uniform along the length of the failure wedge and typically decreased to zero near the wall, although for some tests heave was measured near the wall as well. A photo showing the heave near the wall for one of the non-skew tests is provided in Figure 4-16. This heave near the wall typically was observed to be between 0 and 12 mm (0 and 0.5 in).

Figure 4-16: Photos of Ground Surface Heave near the Backwall for both a Non-Skew and 45° Skew Test

4.5 Displacement and Strain within the Failure Wedge

Plots of the normalized longitudinal ground surface displacement as a function of distance behind the wall are shown in Figure 4-17 at the peak passive force for the tests at the four skew angles. The displacement is normalized by the maximum displacement of the wall. No trends were observed with skew angle. Based on this data, the average compressive strain was computed as a function of distance behind the wall. The average compressive strain is plotted as a function of distance from the back of the wall for an average wall displacement of 16 mm (0.62 inch) or 0.025*H* (typical displacement at peak load) in Figure 4-18. These results indicate that the failure "wedge" does not simply move as a block but undergoes significant compression. As indicated previously, compressive strain is highest in the sand directly behind the wall but decreases with distance. Compressive strains are as high as 8% near the wall but decrease to around 4% at 1 m (3.3 ft) behind the wall.

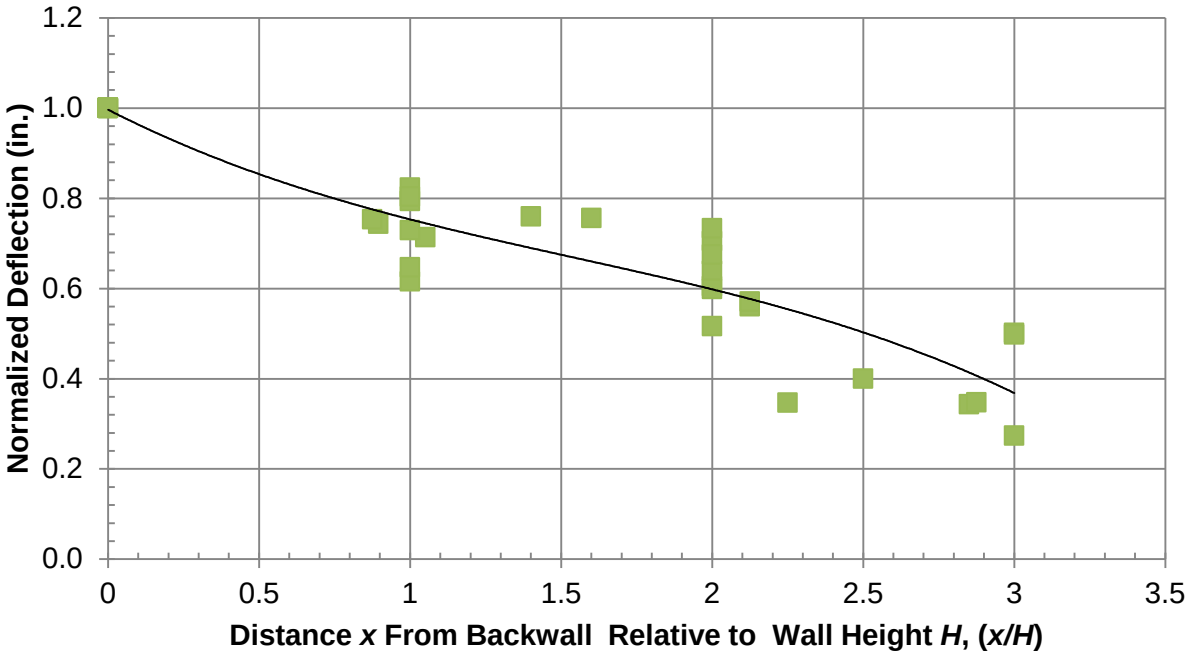

Figure 4-17: Plot of Longitudinal Ground Surface Displacement as a Function of Distance Behind the Wall for Various Skew Angles

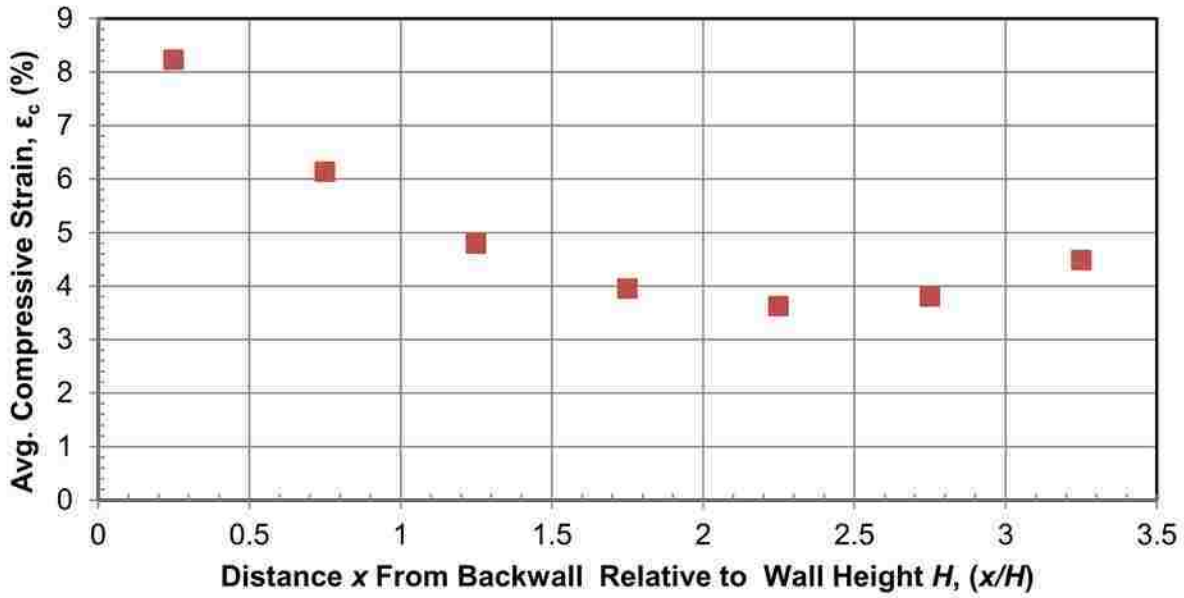

Figure 4-18: Average Compressive Strain as a Function of Distance Behind the wall Based on Ground Surface Displacement Measurements for all Tests

5 ANALYSIS OF TEST DATA

The passive force-deflection curves were computed using the log-spiral method as implemented in the computer programs PYCAP developed by Duncan and Mokwa (2001) and ABUT developed by Shamsabadi et al. (2007). Due to the relatively planar shape of the failure surface for the non-skew case, analysis of the ultimate passive force was also performed according to the Coulomb (1776) method. This section discusses the inputs and results from these analyses, and an equation for computing the passive force for a given skew angle, based on the limited data presently available, is also given.

5.1 Analysis Input Parameters

A summary of input values used in the PYCAP and ABUT passive force-deflection curve analyses is given in Table 5-1. Because of the plane strain geometry involved in the tests, the friction angle measured in the direct shear test for triaxial conditions ($\phi' = 46^o$) was increased to the plane strain ($\phi'_{PS} = 50^o$) value based on the 2D test geometry. As indicated previously, the friction angle of 50° is also consistent with the value obtained from the average inclination of the failure plane. The wall friction angle was taken as 33.2º based on interface friction tests, and Poisson's ratio was taken as 0.3 which is a typical value for dense sand (Budhu, 2007). The average moist unit weight was taken as 18.82 kN/m^3 (120.0 lb/ft^3) based on the nuclear dry density results and the post-testing moisture contents.

Table 5-1: Summary of Input Parameters Used for PYCAP and ABUT Analyses

Parameter	Analysis Method	
	PYCAP (Duncan & Mokwa, 2001)	**ABUT** (Shamsabadi et al, 2007)
ϕ (°)	50	50
δ (°)	33.2	33.2
c (psf)	80	130
v	0.2	0.2
E_i (ksf)	1,000	-
Δ/H	0.03	-
ε_{50}	-	0.004

For the PYCAP analysis initial estimates of the soil elastic modulus E_i were made based on a range recommended by Duncan and Mokwa for dense compacted sand (E_i = 28.8 to 57.5 MPa [600 to 1200 ksf]), but were adjusted by trial and error to a value of 48 kPa (1000 ksf) to obtain improved agreement with the measured curve shape. The back-calculated value is near the middle of the range. The apparent soil cohesion was taken as 4 kPa (80 psf) based on the suction measurements. The normalized displacement at failure was taken as 0.03H based on the test results which is within the 0.03 to 0.05H range recommended by Cole and Rollins (2006) and Caltrans (2001).

For the ABUT analysis initial estimates of the ε_{50} were made based on the range of recommended values (0.002 to 0.003) provided by Shamsabadi et al (2007); however, this value was adjusted by trial and error to a value of 0.004 to improve agreement with the measured curve shape. The apparent cohesion was slightly increased to 6.2 kPa (130 psf) for the ABUT analysis in order to achieve good agreement with measured curves. All other parameters were the same as those indicated previously for the PYCAP analysis.

5.2 Analysis of Results

A comparison of the measured and computed passive force-deflection curves according to the PYCAP and ABUT methods for the no-skew case is provided in Figure 5-1. The agreement between the measured curve and the two computed curves is relatively good. It should be noted that for the relatively shallow depth of soil involved in these tests and for most bridge abutments, the apparent cohesion used in the analysis is a particularly important parameter. For example, the apparent cohesion in accounts for approximately 25% of the computed passive force according to the PYCAP analysis, and approximately 40% according to the ABUT analysis. Therefore, an accurate assessment of this parameter is particularly important for determining the passive force on a bridge abutment under field conditions, and suction measurements could be particularly helpful in selecting a reasonable value.

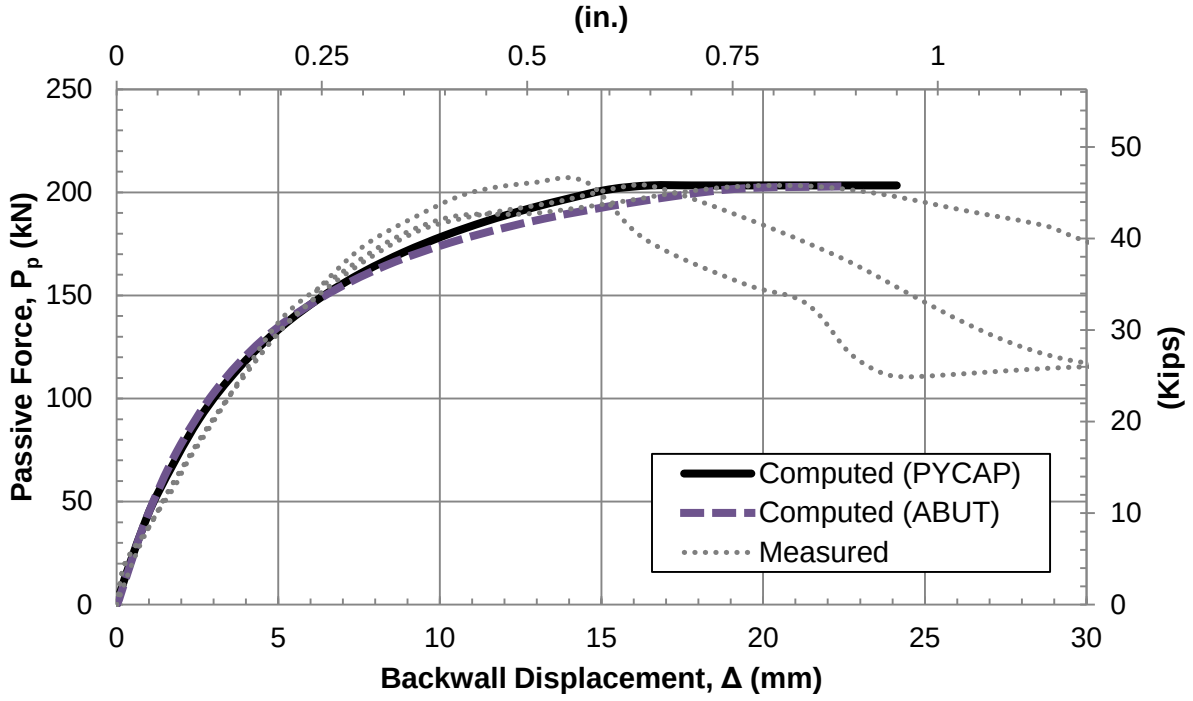

Figure 5-1: Comparison of Measured and Computed Passive Force versus Longitudinal Deflection Curves for the No Skew Case.

5.3 Coulomb Analysis

Because of the relatively linear failure plane observed during the non-skew tests, the test results were also analyzed according to Coulomb Theory for passive pressure. Using the same strength parameters as those used in the PYCAP analysis (ϕ = 50°; δ = 33.2°; c = 80 psf), passive force is overestimated by over 500% using the Coulomb Theory. However, good agreement is achieved using this method when the wall friction angle is decreased to around 0.45ϕ (δ = 23°). The inclination and distance from the wall at the ground surface of the failure surface corresponding to δ = 23° are about 16° and 7 ft, respectively. However, it should be noted that the computed passive force is extremely sensitive to change in wall friction values at this range.

5.4 Skew Equation

The passive force for a given skew angle $P_{P(\text{skew})}$ can be obtained using the equation

$$P_{P(\text{skew})} = P_P R_{\text{skew}} \tag{5-1}$$

where R_{skew} is a reduction factor based on the test results in Figure 4-6 and P_P is the passive force for the no skew case. In all cases, the width of the backwall was taken equal to the width of the actual roadway based on the projected area (no skew case) rather than the actual area along the skew. Based on the limited data presently available, R_{skew} can be computed using the equation

$$R_{\text{skew}} = 8.0 \times 10^{-5} \theta^2 - 0.018\theta + 1.0 \tag{5-2}$$

where θ is the abutment skew angle in degrees. Equation 5-2 is a regression for the test results from this study shown in Figure 4-6. This regression equation has an R^2 value of ___. It should be noted that R_{skew} is applicable only to clean sands, and is based on only one specific wall geometry. It may be that the reduction factor will be dependent on geometric factors such as the width and height of the abutment wall or with differences in soil properties of the backfill. Therefore, it will be important to conduct additional large-scale tests along with calibrated numerical modeling to provide additional guidance to bridge design engineers in the future.

6 SUMMARY AND CONCLUSIONS

6.1 Summary

Passive pressures are important for bridge abutments subjected to thermal expansion and seismic forces, but no test results have been available for skewed abutments. Due to limited understanding of the effect of skew on passive pressures, a series of large-scale lateral load tests were performed on a 1.26 m (4.13 ft) wide and 0.61 m (2 ft) tall backwall with skew angles of 0°, 15°, 30°, and 45°. At least two tests were performed for each skew angle to evaluate repeatability. The backfill material was a poorly-graded clean sand having a plane strain friction angle ϕ of about 50° with an apparent cohesion due to matric suction of approximately 4-5 kPa (70-90 psf).

6.2 Conclusions

Conclusions from this study include the following:

1. Lab tests and numerical analyses indicate that the peak passive force for a skewed abutment decreases significantly as the skew angle increases. Based on available results, the reduction in passive force can be accounted for by using a simple reduction factor. The reduction may be dependent on abutment geometry and other unknown factors; therefore, additional large-scale tests and calibrated numerical analyses would be desirable to provide additional guidance to designers.

2. For the dense compacted sand typical of approach fills for bridges, the peak passive force for both skewed and non-skew tests typically developed at longitudinal deflections between 0.02 and 0.035 times the wall height, *H*. However, the shape of the passive force-deflection curve up to the peak value transitioned from a typical hyperbolic shape for the no skew case to a more bi-linear shape with a relatively flat slope leading to the peak for tests involving skews.
3. At wall displacements beyond the peak passive resistance (0.04 to 0.06*H*) the passive force decreased substantially and the residual or ultimate force was typically about 40% below the peak force, and remained relatively constant with increasing deflection. As the skew angle increased, the drop off in passive force appeared to be more abrupt than for the no skew cases.
4. Lateral movement was typically very small due to the good amount of sliding resistance, which was typically greater than the applied shear force for skew angles up to about 30°.
5. Using measured soil properties such as moist unit weight, plane strain soil friction angle, apparent soil cohesion, and wall friction, two computer models based on the log-spiral approach were successful in computing a peak passive force that was comparable to the measured force for the no skew case. However, for skewed abutments it was necessary to use a reduction factor to obtain a passive force comparable to the measured value.
6. An accurate assessment of the measured passive force for the partially saturated backfill required the determination of the apparent cohesion provided by the suction

in the sand. This apparent cohesion provided a significant percentage (26%) of the computed passive force.

7. The failure “wedge” did not simply move as a rigid block. Significant compressive strains (4 to 8%) occurred within the failure mass near the wall which decreased with distance from the wall.

6.3 Recommendations for Future Research

Although the agreement between the numerical and physical test results suggests the potential for a simple adjustment factor to account for skew effects, it is not certain that this would apply to full scale conditions. Considering the significant apparent decrease in capacity with increasing skew angle, these large-scale test results should be verified with full-scale field tests with varying abutment geometry and possibly backfill type. Thus, it is recommended that additional testing on a full-scale wall be performed. Increasing the wall height will provide conditions where soil unit weight is a greater contributor to backfill passive resistance. Increasing the wall length will provide conditions where 3D effects can be further minimized.

REFERENCES

AASHTO. (2011). Guide Specifications for LRFD Seismic Bridge Design, 2nd Edition.

Brinch Hansen, J. (1966). *Resistance of a rectangular anchor slab*. Copenhagen: Danish Geotechnical Institute.

Budhu, M. (2007). *Soil Mechanics and Foundations, 2nd Ed.* Hoboken, NJ: John Wiley & Sons, Inc.

Burke, M. P. (1994). Semi-Integral Bridges: Movements and Forces. *Transportation Research Record: Journal of the Transportation Research Board, 1460*, 1-8.

CALTRANS. (2001). Seismic design criteria version 1.2. Sacramento, California. : California Department of Transportation.

CALTRANS. (2010). Seismic Design Criteria, ver. 1.6: CALTRANS, Division of Engineering Services, Office of Structure.

Chen, C. S., & Su, J. J. (1994). *A method for passive pressure earth computation on sands.* Paper presented at the 8th International Conference on Methods and Advancements in Geomechanics, Rotterdam, The Netherlands.

Cole, R. T., & Rollins, K. M. (2006). Passive Earth Pressure Mobilization during Cyclic Loading. *Journal of Geotechnical and Geoenvironmental Engineering, 132*(9), 1154-1164.

Coulomb, C. A. (1776). Essai sur une application des regles des maximis et minimis a quelques problemes de statique relatifs a l'architecture. *Memoires de l'Academie Royale pres Divers Savants, 7*.

Duncan, J. M., & Mokwa, R. L. (2001). Passive Earth Pressures: Theories and Tests. *Journal of Geotechnical and Geoenvironmental Engineering, 127*(3), 248-257.

Dunker, K. F., & Liu, D. (2007). Foundations for Integral Abutments. *Practice Periodical on Structural Design and Construction, 12*(1), 22-30.

Khodair, Y. A. (2009). Lateral earth pressure behind an integral abutment. *Structure and Infrastructure Engineering, 5*(2), 123-136.

Kramer, S. L. (1996). *Geotechnical Earthquake Engineering*. Upper Saddle River, New Jersey: Prentice Hall.

Kulhawy, F. H., & Mayne, P. W. (1990). Manual on estimating soil properties for foundation design *Research Project 1493-6, EL 6800*. Palo Alto, California: Electric Power Research Institute.

Kumar, J., & SubgaRao, K. S. (1997). Pasive pressure coefficients, critical failure surface and its kinematic admissability. *Geotechnique, London, 47*(1), 185-192.

Lemnitzer, A., & Ahlberg, E. R. (2009). Lateral performance of full-scale bridge abutment wall with granular backfill. *Journal of Geotechnical and Geoenvironmental Engineering, 135*(9), 506-514.

Likos, W. J., Wayllace, A., & Ning, L. (2010). Direct shear apparatus for unsaturated sands at low suction and stress. *Geotechnical Testing Journal, ASTM*(33), 5.

Maroney, B. H. (1995). *Large scale abutment tests to determine stiffness and ultimate strength under seismic loading.* Ph. D. Ph. D. Dissertation, University of California, Davis.

Mononobe, N., & Matsuo, H. (1929). *On the Determination of Earth Pressures During Earthquakes.* Paper presented at the World Engineering Congress.

Okabe, S. (1926). General Theory of Earth Pressures. *Journal of the Japan Society of Civil Engineering, 12*(1).

Ovesen, N. K. (1964). *Anchor slabs, calculation methods, and model tests*. Copenhagen, : Danish Geotechnical Institute.

Potyondy, J. G. (1961). Skin friction between various soils and construction materials. *Geotechnique, London, 11*(1), 339-353.

Rankine, W. J. (1857). On the stability of loose earth. *Philosophical Transactions of the Royal Society of London, 147*.

Rollins, K. M., & Cole, R. T. (2006). Cyclic Lateral Load Behavior of a Pile Cap and Backfill. *Journal of Geotechnical and Geoenvironmental Engineering, 132*(9), 1143-1153.

Rollins, K. M., & Sparks, A. (2002). Lateral Resistance of Full-Scale Pile Cap with Gravel Backfill. *Journal of Geotechnical and Geoenvironmental Engineering, 128*(9), 711-723.

Sandford, T. C., & Elgaaly, M. (1993). Skew effects on backfill pressures at frame bridge abutments. *Transportation Research Record: Journal of the Transportation Research Board, 1415*, 1-11.

Shamsabadi, A., Kapuskar, M., & Zand, A. (2006). *Three-Dimensional Nonlinear Finite-Element Soil-Abutment Structure Interaction Model for Skewed Bridges*. Paper presented at the Fifth National Seismic Conference on Bridges & Highways, San Francisco, CA.

Shamsabadi, A., Rollins, K. M., & Kapaskur, M. (2007). Nonlinear Soil-Abutment-Bridge Structure Interaction for Seismic Performance-Based Design. *Journal of Geotechnical and Geoenvironmental Engineering, 133*(6), 707-720.

Soubra, A. H. (2000). Static and seismic earth pressure coefficients on rigid retaining structures. *Canadian Geotechnical Journal, 37*, 463-478.

Steedman, R. S., & Zeng, X. (1990). *The Seismic Response of Waterfront Retaining Walls*. Conference Proceedings, ASCE Specialty Conference on Design and Performance of Earth Retaining Structures, (25). Cornell University, Ithaca, New York.

Steinberg, E., & Sargand, S. (2010). *Forces in Wingwalls from Thermal Expansion of Skewed Seimi-Integral Bridges*. (FHWA/OH-2010/16). Athens, OH: Ohio Department of Transportation.

Steinberg, E., Sargand, S. M., & Bettinger, C. (2004). Forces in Wingwalls of Skewed Semi-Integral Bridges. *Journal of Bridge Engineering, 9*(6), 563-571.

SubbaRao, K. S., & Choudhury, D. (2005). Seismic Passive Earth Pressures in Soil. *Journal of Geotechnical and Geoenvironmental Engineering, American Society of Civil Engineers, 131*(1), 131-135.

Terzaghi, K. (1943). *Theoretical Soil Mechanics*. New York: Wiley.

Terzaghi, K., & Peck, R. B. (1996). *Soil mechanics in engineering practice, 3rd Edition*. New York: Wiley.

Zhu, D. Y., & Qian, Q. (2000). Determination of Passive Earth Pressure Coefficient by the Method of Triangular Slices. *Canadian Geotechnical Journal, 37*(2), 485-491.